Calculated and Measured Doppler Hydrogen Line Profiles at Arbitrary Angles with the Magnetic Field

by
Fred Sigernes

Cand. Scient. Thesis
University of Tromsø
November 1991

Acknowledgments

Firstly, I would like to thank Dr. Kjell Henriksen for teaching me fundamental principles and practical skills involved in the field of experiemental and teoretical spectrophysics. Thanks are also due of fellow student **Dag Lorentzen** for numerous helpful discussions of the subject presented.

Secondly, I wish to thank the students for their criticism and support of this work. They are Geir Arne Hansen, Trond Svenøe, Frank Øynes, Stefan Claes, Tryggve Sparr, Tryggve Sørensen, Arve Kylling and Eirik Malnes .

Thirdly, I would like to thank Drs. Ilja Kornilov, Viktor Golubsov, Roger Smith, Charles Deehr, Robert M. Hamwey, Galine Totunova, Boris Kozelov, Joe Minow, Jim Conner and Gina Price for cooperation and for teaching me observational techniques.

A special thanks goes to my girlfriend Gerd Irene Andersen and my family for all their encouragements and understanding during this work.

At last, but not at least I wish to thank my friends, all fellow students, The Student House, Mack Brewery and Ruphus Student Club for keeping me busy during non–scientific moments.

Contents

List of Figures

List of Tables

Chapter 1

Introduction

Auroral protons that are entering the atmosphere will change between being protons or neutral hydrogen atoms. A proton can either capture or loose an electron when it is penetrating into the atmosphere. This charge exchange process gives raise to a diffuse aurora called the proton aurora, which normally consists of Doppler shifted and broadened hydrogen line profiles. Our task is to calculate and measure these Doppler shifted line profiles, H_α and H_β, at arbitrary view angles to the magnetic field. The calculations are two–dimensional and the measurements are carried out with two Ebert-Fastie spectrometers.

The first indications of proton aurora was published by *Vegard* (1939). He found out that the source of the proton aurora was protons originating from the solar wind. Since this discovery there has been a considerable number of papers written on this subject. The literature was reviewed by *Chamberlain* (1961) and *Galperin* (1963). *Eather et al.* (1965) published measured auroral hydrogen profiles using a photometer with a tilting interference filter. Relative little work has been published since then, especially when it comes to modelling of Doppler shifted line profiles. Recent measurements made by satellites and rockets of proton energy spectra encourage us to construct a numerical model trying to understand and explain the not yet well understood Doppler shifted and broadened hydrogen line profiles, compare the results of the model with measurements and thus maybe reveal some of the secrets of the proton aurora.

Chapter 2

Energy loss of protons travelling through the atmosphere

"Probably the best way of obtaining rates of energy loss from present data is to differentiate empirical relations for this purpose", obtained from *Cook et al.* (1953).

In this chapter we will try to calculate how a given proton energy distribution at the top of the atmosphere changes as a function of height in the atmosphere. The calculation is two dimensional and, the proton energy spectrum is assumed to be a narrow beam of incoming particles. A semi–empirical range relation of protons in air is used to calculate energy loss. The cross sections for charge exchange of protons and hydrogen atoms with other atmospheric constituents dominate over competing cross sections. Picking up or releasing an electron has little influence on the momentum of the protons, and therefore the pitch-angle is negligible changed during each collision or charge exchange process.

2.1 Range of protons

2.1.1 Definition of range

Range R of a proton can be defined as the length the proton penetrates when it is shot with initial energy E into a gas with mass density ρ, and expressed as :

$$R(E) = \int_0^E \rho \cdot \left(\frac{-dE}{dx} \right)^{-1} dE \qquad (g/cm^2), \tag{2.1}$$

where E is energy of the proton (eV), R range of a proton in a gas with mass density ρ (g/cm^3), and x length in cm the proton travels.

2.1.2 The range–pitch-angle relation

A proton with energy, E, goes through numerous charge exchanges with atmospheric atoms and molecules before it ends as a thermic hydrogen atom. For energies less than 30 keV the main part of the precipitated particles travel as hydrogen atoms and for energies higher than 30 keV as protons (*Bernstein et al.*, 1969). The proton can either capture an electron or loose one when it is travelling through the atmosphere. This charge exchange is shown in Fig. 2.1.

We are now introducing the pitch-angle, θ, and are further assuming that the pitch-angle is constant when the proton travels through the atmosphere. It means, a proton and the associated hydrogen atom will have the same pitch angle at the top of the atmosphere as further down, before it gets thermalized. The travelling distance down to a height h is the same whether the particle is charged or neutral, assuming that the magnetic field is parallel and vertical. See Fig. 2.2.

The range relation can be transformed into an expression more adequate for numerical calculations.

$$R(E) = \int_0^E \rho \cdot \left(\frac{-dE}{dx} \right)^{-1} dE = \int_H^h \rho(x) dx \approx \sum_{x=H}^{h} \rho(x) \Delta x.$$

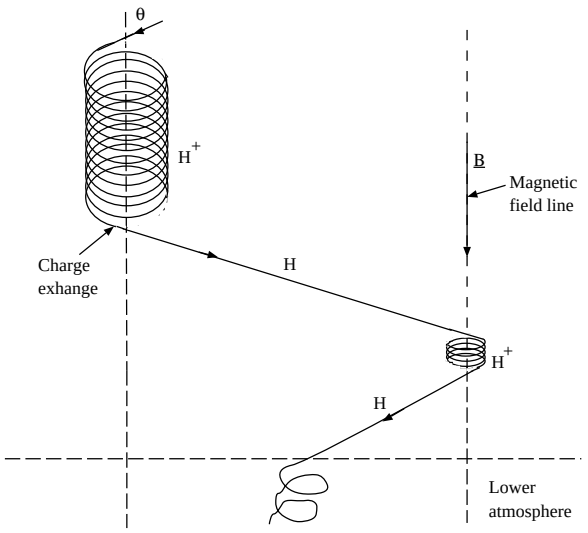

Figure 2.1: Path of a proton shot into the atmosphere, θ pitch–angle and $\underline{B}$ vector of the geomagnetic field.

Introducing :

$$H - h = xcos(\theta) \Rightarrow dx = \frac{-dh}{cos(\theta)},$$

then

$$R(h,\theta) \approx \left(\frac{1}{cos(\theta)}\right) \cdot \sum_{h=h'}^{H} \rho(h')\Delta h', \tag{2.2}$$

where H is the height at the top of the atmosphere, and h an arbitrary height in the atmosphere. The range relation is visualized in Fig. 2.3 for several pitch-angles.

We see that if the pitch-angle is increasing, the protons will penetrate shorter into the atmosphere. Using a pitch-angle relation, the necessary energy of protons at the top of the atmoshpere can be calculated in order to reach down to a certain height h. The mass density as a function of height from 600 km down to 90 km can be obtained from the Msis–86 model (*Hedin*, 1987).

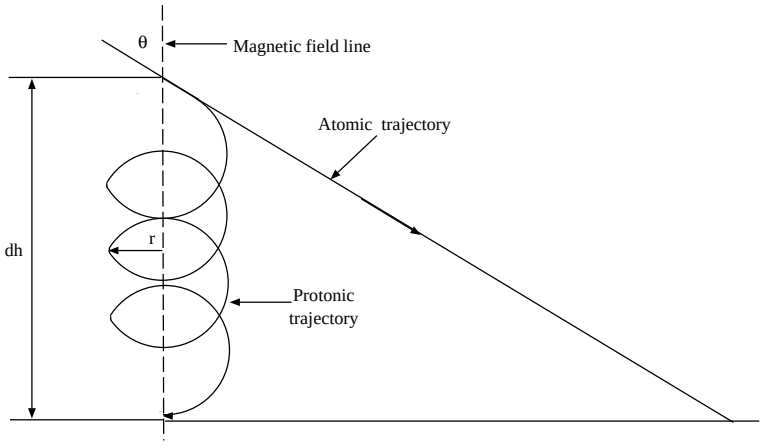

Figure 2.2: The path of a spiralling proton and a hydrogen atom.

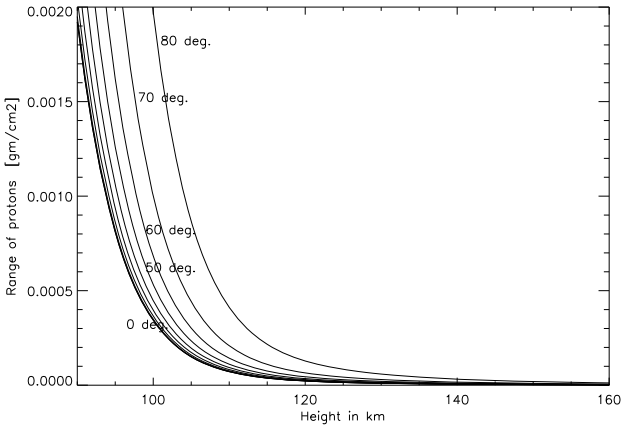

Figure 2.3: The range-pitch-angle relation. Each curve represents the range for protons with initial pitch–angle between 0 to 80 degrees.

2.1.3 Experimental range of protons in air

We have used the experimental data of protons in air obtained by *Cook et al.* (1953). They are displayed in Fig. 2.4.

The range is obtained when the temperature in the air is $15°C$ and the pressure 1mmHg. From the ideal gas law $\rho = \frac{m}{kT}p$ and the mean molecular mass m=$4.81{\cdot}10^{-23}$ g, we find that $1mmHg - cm = 1.61{\cdot}10^{-6} g/cm^2$, when T=288 K, k=$1.38{\cdot}10^{-23}$ J/K and p=1mmHg=$1.33{\cdot}10^{2}$ Pa. Fig. 2.4 shows how far a proton can reach in air with

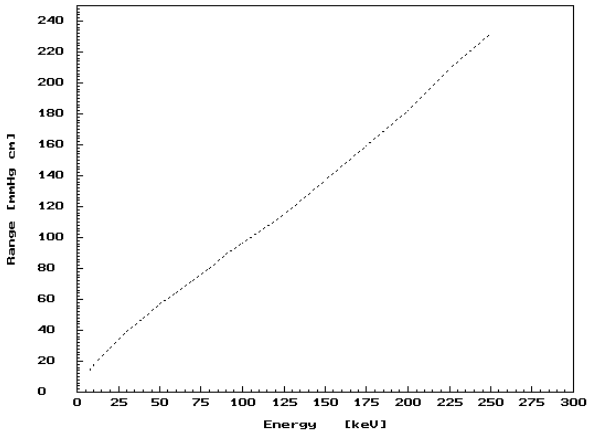

Figure 2.4: Experimental range of protons in air (*Cook et al.*, 1953).

energy E.

The relation between the range R and the energy E can be approximated with the expression :

$$R(E) = \begin{cases} kE^n & E < E_0 \\ C(E + E_1)^{1.5} & E > E_0. \end{cases} \tag{2.3}$$

The parameters k, C, E_1 and n are chosen to fit the experimental data. E_0 is the energy when the rate of the energy loss is maximum. The values of the fitted parameters are : k=3.26 cm/$(keV)^n$, C=0.0393 cm/$(keV)^{1.5}$, n=0.73, E_0=76.5 keV, and E_1=80.0 keV. Using these values, a good fit to the experimental data is obtained and shown in Fig. 2.5.

2.2 Energy loss

2.2.1 The energy-range relation

Using energy-range relation of protons in air from equation (2.3) :

$$R(E) = \begin{cases} kE^n & E < E_0 \\ C(E + E_1)^{1.5} & E > E_0, \end{cases}$$

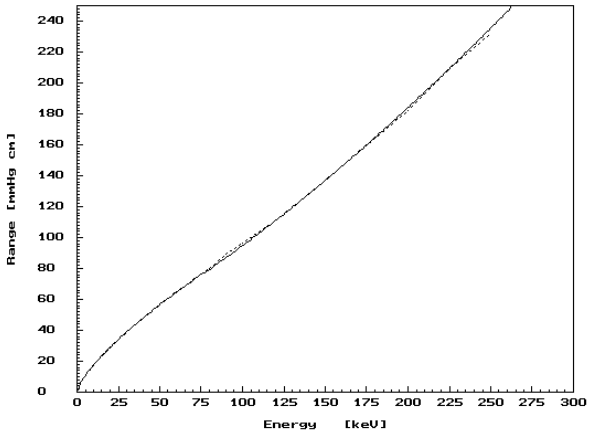

Figure 2.5: Fit of experimental data to the above energy–range relation

where the range is given in mmHg-cm and the energy in keV, the energy degradation can now be found by derivation.

$$\frac{dE}{dR} = \begin{cases} \frac{1}{nk} E^{-n+1} & E < E_0 \\ \frac{2}{3C}(E + E_1)^{-0.5} & E > E_0. \end{cases}$$

It is now possible to use this to calculate the energy loss of a proton from an upper level at height H down to a certain height h (*Henriksen*, 1978) :

$$\Delta E(h, \theta) = \left(\frac{1}{cos(\theta)}\right) \cdot \sum_{h=h'}^{H} \left(\frac{dE}{dR}\right) \cdot \left(\frac{\rho(h')}{\rho_0}\right) \Delta h'. \tag{2.4}$$

E is the instantaneous energy,

$$E = E(h, \theta) = E(H, \theta) - \Delta E(h, \theta). \tag{2.5}$$

$E(H, \theta)$ is the initial energy at height H, θ the pitch-angle of the protons, $\rho(h)$ the mass density at height h and ρ_0 the mass density with pressure 1mmHg and temprature 288 K. The energy degradation is calculated in intervals of $\Delta h = 1$ km, and the total energy loss $\Delta E(h, \theta)$ is found by adding up the energy degradation at each height interval above height h.

The protons are assumed to spiral with constant pitch-angle and travel in straight lines when neutralized. The stopping power of the atmosphere varies as $\frac{1}{cos(\theta)}$. The travelling distance down to height h is the same whether the particle is charged or

neutral, the magnetic field is parallel and vertical, and this relation is shown in Fig. 2.6.

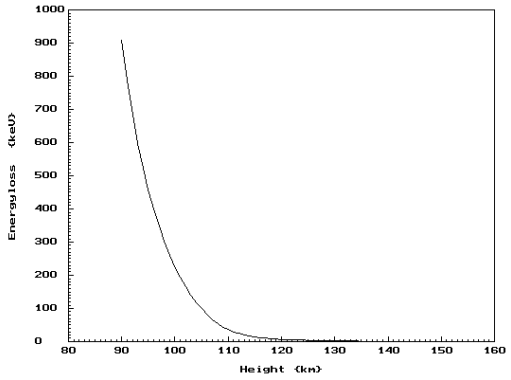

Figure 2.6: Energy loss of protons in the atmosphere with pitch-angle equal to zero, when the magnetic field is vertical and parallell.

The travelling distance is the same since in spiralling and straight line running the pitch-angle is equal in both cases. We can see that a proton penetrating into the atmoshere with pitch–angle equal to zero will not loose much energy before it reaches down to a height of about 120 km. Above this height the loss becomes negligible, less than 1 keV. At 100 km the energy loss is about 200 keV.

2.2.2 The pitch-angle distribution

Since E is a function of θ and h, the energy must be calculated for each θ at height h. When $E \leq 0$, there are no protons travelling in the dircetion of θ at height h. E is the directed kinetic energy, associated with the velocity fixed in the θ direction. Therefore the kinetic energy can never be negative.
We now introduce a θ_h given by

$$E(h, \theta_h) = 0. \tag{2.6}$$

When $|\theta| < \theta_h$, then $E(h, \theta) > 0$, and when $|\theta| > \theta_h$, then $E(h, \theta) = 0$.
Since energy is lost downwards, θ_h must decrease as h decreases. Fig. 2.7 shows

how θ_h varies with height and initial energy. We assume the maximum initial energy at the top of the atmosphere to be 1MeV. It is then necessary to calculate θ_h at each arbitrary height h and initial energy, from the equation $E(h, \theta_h) = 0$. Then we would know how the pitch-angle distribution, $n(h, \theta)$, is for each h, when the initial energy is given.

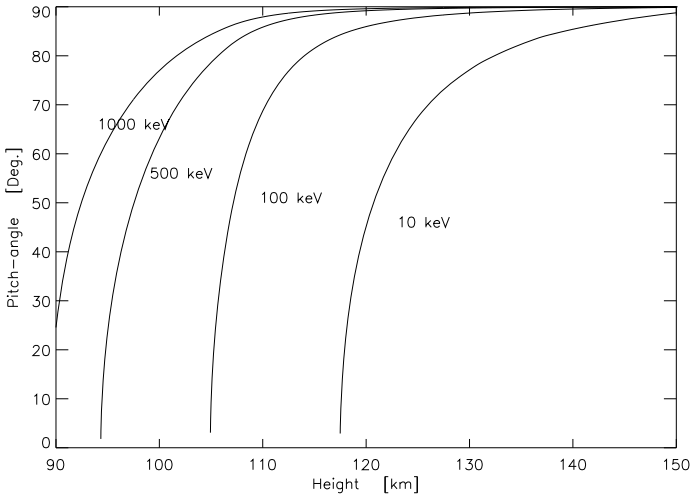

Figure 2.7: θ_h as a function of h for protons with initial energies of 1000, 500, 100 and 10 keV

Introducing the integrated function of the pitch-angle distribution :

$$N(h, \theta_h) = \int_{-\theta_h}^{+\theta_h} n(h, \theta) d\theta. \tag{2.7}$$

The pitch-angle distribution, $n(H, \theta)$, can be normalized at the top of the atmosphere

$$N(H, \theta_H) = 1,$$

where $\theta_H = \frac{\pi}{2}$ and $n(\theta) = \frac{1}{2} \cdot cos(\theta)$.
We assume that the pitch-angle distribution is independent of energy at the top of the atmosphere, something that is not necessarily true, but in lack of data concidering this problem we assume this to be a reasonable assumption. The pitch-angle distribution becomes more and more narrow as the protons penetrate deeper into the atmosphere. At 150 km the distribution is defined within the range from about $-90°$ to $+90°$, but at 90 km this range is just from $-25°$ to $+25°$ for protons with initial energy 1 MeV. This, because the protons with pitch-angles larger than θ_h will be stopped before they reach height h.

2.2.3 The energy distribution at an arbitrary height in the atmosphere

If we know the energy distribution at the top of the atmosphere, $f(E(H,\theta))$, it is possible to calculate how this distribution changes as a function of height, $F(E(h,\theta))$, by the following expressions :

$$F(E(h,\theta)) = F(E(H,\theta) - \Delta E(h,\theta)) = f(E(H,\theta)) \cdot n(h,\theta). \tag{2.8}$$

$F(E(h,\theta))$ is the flux of protons travelling in the direction of θ at heigth h, and $\theta \in [-\theta_h, +\theta_h]$ with energy $E(h,\theta)$. This number is identical to $F(E(H,\theta))$ at the top of the atmosphere, but the energy of the protons is of course less at height h. Using measurements of energy distribution of protons at the top the atmosphere, (*cf. Vallance Jones*, 1974), see Fig. 2.8, these data can be approximately given by the following function :

$$f(E(H,\theta)) \approx \begin{cases} a \cdot E(H,\theta)^{-b} & 0.2 \leq E(H,\theta) \leq 3.6 \\ N_0 \cdot E(H,\theta) \cdot e^{-E(H,\theta)/9} & E(H,\theta) > 3.6, \end{cases} \tag{2.9}$$

where the unit of $E(H,\theta)$ is keV.

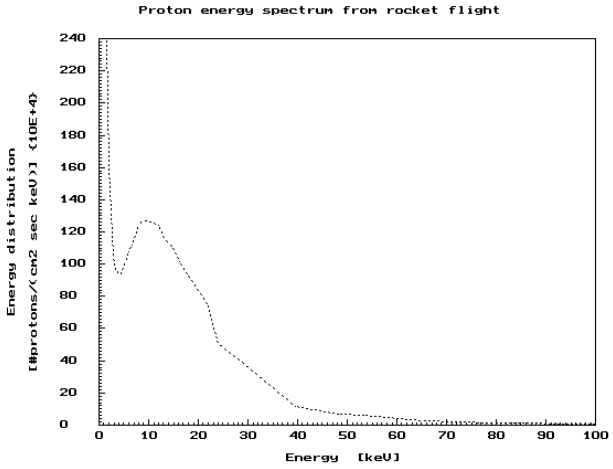

Figure 2.8: Measured proton energy spectrum in the recovery phase aurora (*Reasoner et al.*, 1968).

Fitting these expressions to the data from *Reasoner et al.* (1968), the best fit is obtained when the parameters have the following values : $a = 7.97 \cdot 10^5$, $b = 1.31$, and $N_0 = 6.0 \cdot 10^4$. The data and the best fit is shown in Fig. 2.9.

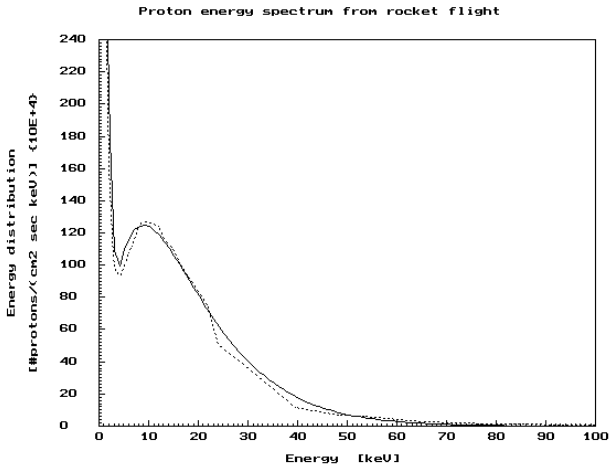

Figure 2.9: Measured proton spectrum as above, dotted curve, and the fitted analytical spectrum, solid curve.

We are assuming that $f(E(H,\theta))$ is independent of time. The average value of $E(h,\theta)$ within the range $[-\theta_h, +\theta_h]$ and the corresponding value of the total flux, integrated over the pitch–angles, at height h can be calculated according to the expressions :

$$\overline{E(h)} = \frac{1}{2\theta_h} \int_{-\theta_h}^{+\theta_h} E(h,\theta) d\theta \tag{2.10}$$

and

$$F_T(\overline{E(h)}) \approx \int_{-\theta_h}^{+\theta_h} F(E(h,\theta)) d\theta.$$

$F_T(\overline{E(h)})$ is the distribution of the total proton flux as function of energy and is shown in Fig. 2.10. The energy distribution at 150 km is obtained from the measurements of *Reasoner et al.* (1968).

Calculations show that the above proton spectrum does not change shape at heights above 150 km, because there is no significant energy loss of the penetrating protons. At heights lower than 150 km the proton spectrum changes, especially the low energy tail, which is described at the top by $a \cdot E^{-b}$. This tail will be connected

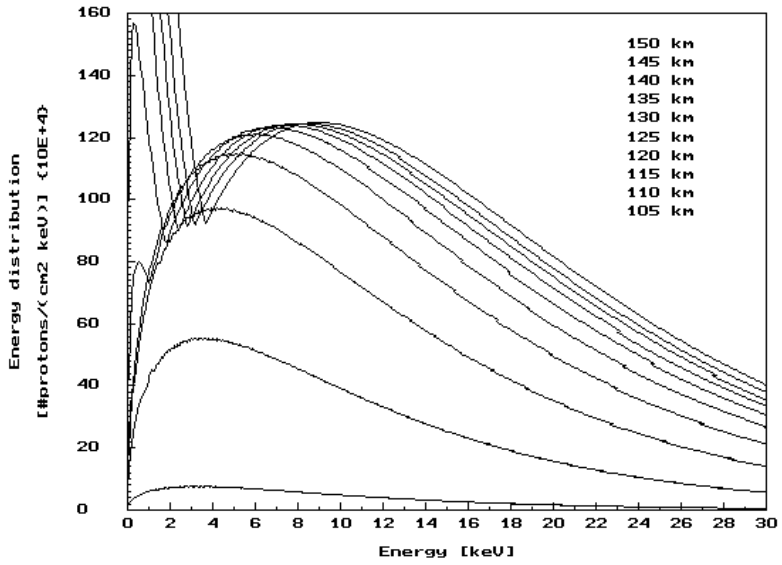

Figure 2.10: Calculated energy distributions. Each curve represents the distribution at one height between 150 km and 90 km, and one curve is shown for each fifth km.

to the Maxwellian-like distribution as an additional low-energy peak. The protons will start to loose energy around 150 km and at $h \approx 127$ km the low-energy peak has disappeared. The low energy protons are stopped faster than those with higher energy. We can also see that the high energy Maxwellian–like proton distribution is shifted towards lower energies when the height decreases. The initial proton flux has completely vanished at heights lower than $h \approx 104$ km.

Chapter 3

The effective emission rate of energetic hydrogen atoms

This chapter will review the collision processes that are involved when protons enter the atmosphere. The most important are charge exchange processes. Protons that are entering the atmosphere will change between protons, H^+, and neutral hydrogen atoms, H. The status of this charge exchange can be given by the flux fraction. The total number of the penetrating particle flux consists of protons and hydrogen atoms, and if we know the fraction of hydrogen atoms, which depend on energy, the effective emission rate can be calculated.

The calculations in the first part of this chapter is based on *Omholt* (1971).

3.1 Charge exchange

3.1.1 Collision processes

When a proton enters the atmosphere it will loose energy in the form of inelastic collisions, ionization and excitation of atmospheric atoms and molecules. The capture of an electron can be described by the following process :

$$H^+ + M \rightarrow H + M^+, \tag{3.1}$$

where M stands for atmospheric atoms or molecules. The hydrogen atom can either be in the ground level or in an excited state. If it is excited, emissions like H_α and H_β will occur before it is back in the ground state. The hydrogen atom will then travel in a straight line unaffected of the magnetic field until it looses the captured electron. Then the proton is spiralling around the magnetic field line as long as it is in charged state. This process can be described by :

$$H + M \rightarrow H^+ + M + e, \tag{3.2}$$

and the effect of the neutralization and charging processes on the incoming particle is shown in Fig. 2.1.

3.1.2 Proton beam approximation

We are now looking at a beam of N_p protons and N_H hydrogen atoms, representing respectively the number of protons and hydrogen atoms per unit area, penetrating the atmosphere. σ_{10} represents the cross section for capture of an electron by a proton (3.1), and σ_{01} represents the cross section for loss of an electron by a hydrogen atom (3.2). The change in the number of protons per unit path travelled can then be described by the following equation :

$$\frac{dN_p}{ds} = -N_p \cdot N_M \cdot \sigma_{10} + N_H \cdot N_M \cdot \sigma_{01}. \tag{3.3}$$

N_M is the concentration of atmospheric atoms and molecules. The terms on the right side of equation (3.3) represent loss and production of protons, respectively.

3.1.3 Flux fractions

When considering the flux fractions in detail, several relations have to be defined.

$$N_M ds = dS \quad and \quad N = N_H + N_p = constant.$$

S is the number of atoms and molecules per unit area the particle traverses along the track through the atmosphere. ds is an inifinitesimal length of this path. The flux fractions for respectively protons and hydrogen atoms are defined as :

$$F_p = \frac{N_p}{N} \quad and \quad F_H = \frac{N_H}{N}.$$

Then we obtain from equation (3.3) :

$$\frac{dF_p}{dS} = -F_p\sigma_{10} + F_H\sigma_{01}$$

or

$$\frac{dF_p}{dS} = -\frac{dF_H}{dS}.$$

If we now regards σ_{10} and σ_{01} as constants, we can obtain the following solution :

$$F_p = F_{p\infty} + (F_{p0} - F_{p\infty})e^{-(S-S_0)(\sigma_{01}+\sigma_{10})},$$

where

$$F_{p\infty} = \frac{\sigma_{01}}{\sigma_{01} + \sigma_{10}}$$

and

$$F_p = F_{p0} \quad \text{when} \quad S = S_0.$$

The average distance over which the (H^+/H)-particles suffer one collision of each kind per particle per unit area is defined as $\Delta S = \frac{1}{\sigma_{01}+\sigma_{10}}$. In practice F_p and F_H will be stable after just a few collisions. Then there are left two stable solutions :

$$F_{p\infty} = \frac{\sigma_{01}}{\sigma_{01} + \sigma_{10}} \tag{3.4}$$

and

$$F_{H\infty} = \frac{\sigma_{10}}{\sigma_{01} + \sigma_{10}}.$$

Data considering σ_{10} and σ_{01} as function of energy are obtained from *Van Zyl et al.* (1980). The flux fractions are shown in Fig. 3.1.

We can see that for energies less than 30 keV the (H^+/H)-particle beam consists of mostly hydrogen atoms, but for higher energies the protons will dominate.

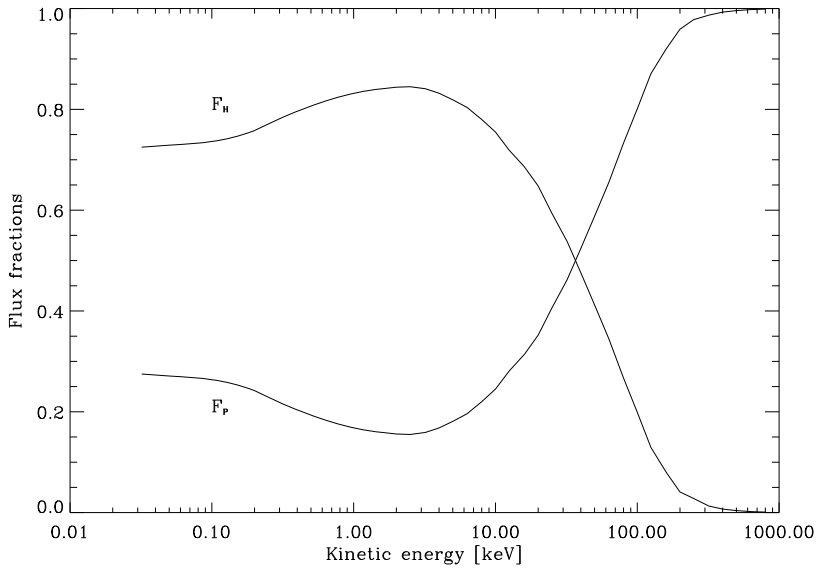

Figure 3.1: The flux fraction for protons $F_p = F_{p\infty}$ and hydrogen atoms $F_H = F_{H\infty}$ as a function of energy.

3.2 Excitation of the hydrogen lines

3.2.1 Statistical equilibrium

At statistical equilibrium the same amount of incoming electrons per unit time to one spesific energy level, n, equals the amount of electrons leaving this level. The simultaneous charge exchange and excitation process can be written as

$$H^+ + M \rightarrow H(n) + M^+ \tag{3.5}$$

and similarly the ionization process

$$H(1) + M \rightarrow H^+ + M. \tag{3.6}$$

H(n) is the hydrogen atom in the n-th energy level, and H(1) is the hydrogen atom in the ground state. At statistical equilibrium the variation of beam particles per unit time in the n-th energy level can be put to :

$$\frac{dN_{H(n)}}{dt} = N_{H(1)} \cdot N_M \cdot \sigma_{01} \cdot \frac{ds}{dt} + N_p \cdot N_M \cdot \sigma_{10} \cdot \frac{ds}{dt} + \sum_{m=n+1}^{\infty} A_{mn} \cdot N_{H(m)} - \sum_{m=1}^{n-1} A_{nm} \cdot N_{H(n)}, \tag{3.7}$$

where A_{mn} is the propability of transmission from the m-th to the n-th energy level, $N_{H(m)}$ - number of hydrogen atoms in the m-th energy level, N_M - concentration of atmospheric atoms or molecules, σ_{01} cross section for the process (3.6), σ_{10} cross section for the process (3.5), and ds - travelled distance during the time interval dt. The two last terms of (3.7) represents respectively transition from higher energy levels down to the n-th level and spontaneous emissions from this energy level to lower levels.

3.2.2 The emission rate

The number of photons emitted per second can be obtained from equation (3.7). Equilibrium is defined by

$$\frac{dN_{H(n)}}{dt} = 0.$$

The velocity of the hydrogen atom is $v = \frac{ds}{dt}$. Solving equation (3.7), gives

$$N_{H(n)} = \frac{1}{\sum_{m=1}^{n-1} A_{nm}} \left(N_{H(1)} \cdot N_M \cdot \sigma_{01} \cdot v + N_p \cdot N_M \cdot \sigma_{10} \cdot v + \sum_{m=n+1}^{\infty} A_{mn} \cdot N_{H(m)} \right).$$

By definition the transition between an upper level n and a lower level m equals

$$I_{nm} = N_{H(n)} \cdot A_{nm},$$

and therefore the emission rate can be written

$$I_{nm} = \frac{A_{nm}}{\sum_{m=1}^{n-1} A_{nm}} \left(N_{H(1)} \cdot N_M \cdot \sigma_{01} \cdot v + N_p \cdot N_M \cdot \sigma_{10} \cdot v + \sum_{m=n+1}^{\infty} A_{mn} \cdot N_{H(m)} \right). \quad (3.8)$$

I_{nm} is the number of fotons emitted per second from the beam of incident protons. Equation (3.8) can be developed and given in terms of the flux fractions

$$I_{nm} = \frac{A_{nm}}{\sum_{m=1}^{n-1} A_{nm}} N_M \cdot \left(N_{H(1)} \cdot \sigma_{01} \cdot v + N_p \cdot \sigma_{10} \cdot v + \frac{1}{N_M} \cdot \sum_{m=n+1}^{\infty} A_{mn} \cdot N_{H(m)} \right)$$

or

$$I_{nm} = \frac{A_{nm}}{\sum_{m=1}^{n-1} A_{nm}} N_M \cdot N \cdot \left(\frac{N_{H(1)}}{N} \cdot \sigma_{01} \cdot v + \frac{N_p}{N} \cdot \sigma_{10} \cdot v + \frac{1}{N_M \cdot N} \cdot \sum_{m=n+1}^{\infty} A_{mn} \cdot N_{H(m)} \right).$$

Since

$$F_{p\infty} = \frac{N_p}{N} \quad \text{and} \quad F_{H\infty} = \frac{N_H}{N},$$

then

$$I_{nm} = \frac{A_{nm}}{\sum_{m=1}^{n-1} A_{nm}} N_M \cdot N \cdot \left((F_{H\infty} \cdot \sigma_{01} + F_{p\infty} \cdot \sigma_{10}) \cdot v + \frac{1}{N_M \cdot N} \cdot \sum_{m=n+1}^{\infty} A_{mn} \cdot N_{H(m)} \right).$$

The effective emission cross section is given by :

$$\sigma_{eff} = F_{H\infty} \cdot \sigma_{01} + F_{p\infty} \cdot \sigma_{10}$$

or

$$I_{nm} = \frac{A_{nm}}{\sum_{m=1}^{n-1} A_{nm}} N_M \cdot N \cdot \left(\sigma_{eff} \cdot v + \frac{1}{N_M \cdot N} \cdot \sum_{m=n+1}^{\infty} A_{mn} \cdot N_{H(m)} \right) \qquad (3.9)$$

Neglecting excitation produced by cascading from higher enegy levels, the emission rate becomes

$$I_{nm} = \frac{A_{nm}}{\sum_{m=1}^{n-1} A_{nm}} \left(N_M \cdot N \cdot \sigma_{eff} \cdot v \right), \qquad (3.10)$$

when $N_{H(1)} >> N_{H(2)} + N_{H(3)} + N_{H(4)} + ...$ The effective emission cross sections when hydrogen atoms collide with N_2 and O_2 are from *Van Zyl et al.* (1980).
See Fig. 3.2

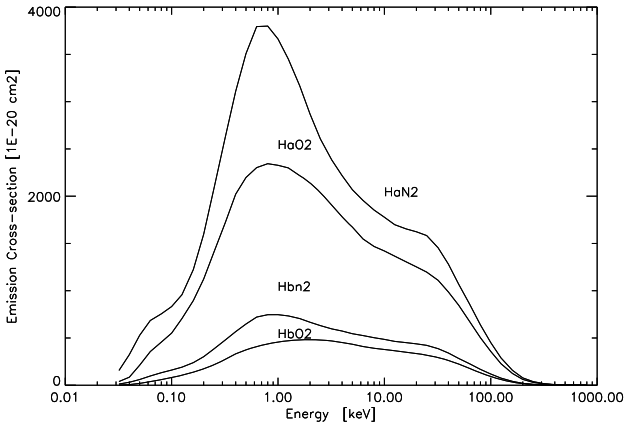

Figure 3.2: The effective emission cross sections for proton collisions in N_2 and O_2 from *Van Zyl et al.* (1980).

We can see from Fig. 3.2 that there is emitted most light for energies of about 1 keV. Then the particles are mostly neutral, but have still a long distance to travel before they end as thermic atoms.

3.2.3 The emission rate at an arbitrary height in the atmosphere

Considering H_α-emissions, that is n=3 and m=2 in equation (3.10), then the emission rate per (H^+/H)-particle is :

$$\varepsilon_{32} = \frac{I_{32}}{N} = \frac{A_{32}}{A_{31} + A_{32}} \left(N_M \cdot \sigma_{eff} \cdot v\right). \tag{3.11}$$

From the previous chapter we found the total flux, $F_T(\overline{E(h)})$, which is the energy distribution of the (H^+/H)-particles at an arbitrary height h. The total emission rate at an arbitrary height can be written as

$$J_{32} = \varepsilon_{32} \cdot F_T(\overline{E(h)}).$$

J_{32} gives the number of photons per unit time and per unit area emitted from a beam of $F_T(\overline{E(h)})$ (H^+/H)-particles at height h. Fig. 3.3 shows J_{32} calculated as a function of the mean energy and different heights.

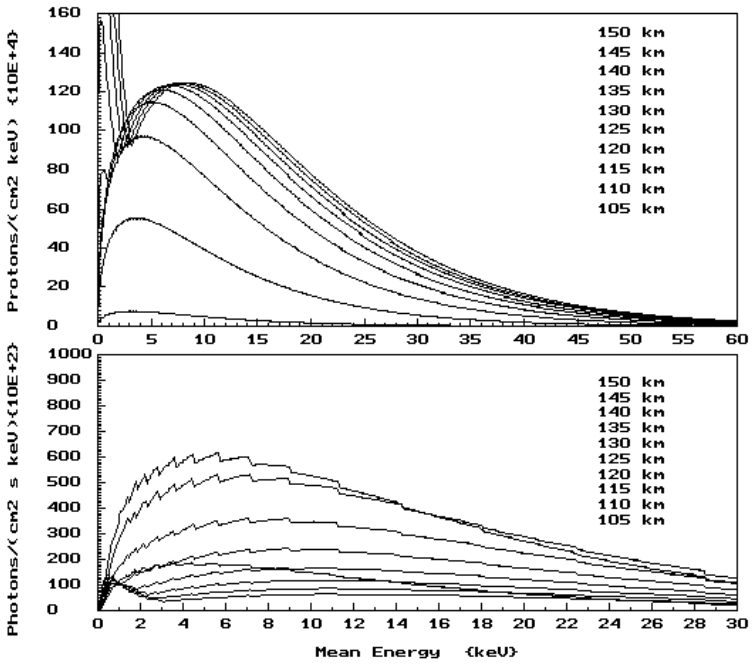

Figure 3.3: The calculated emission rate distribution for different heights

Upper panel of Fig. 3.3 shows the proton distribution at different heights for the proton spectrum measured by *Reasoner et al.* (1968). Lower panel shows the cor-

responding calculated emission rate of H_α related to particle energies for different heights. The low energy tail in the energy distribution will give a corresponding emission peak in the emission distribution for heights over about 127 km, because the low energetic tale of (H^+/H)-particles emits most light. The emission rate distribution will have an increasing maximum shifted towards higher energies, when the (H^+/H)-particles travel further down into the atmosphere. At 115 km, however, the absolute maximum is reached. The maximum of the emission rate distribution will then decrease and be shifted towards lower energies for those (H^+/H)-particles which travel further downwards.

Chapter 4

Modelling of hydrogen line profiles

In this chapter the hydrogen line profiles observed at arbitrary angles to the magnetic field line will be calculated. The observed profiles of H_α and H_β are always Doppler shifted and/or broadened. They are formed by the pitch-angle, energy distribution, scattering angle and energy degradation of the particle influx, and the atmospheric structure. Using these parameters it is possible to make a numerical method, calculating the Doppler profiles integrated over height.

4.1 Basic parameters

The protons are assumed to spiral with constant pitch-angle around field lines and travel in straight lines when neutralized. Therefore the angular distribution is independent of the initial energy.

The assumed pitch-angle distribution, at 600 km in the upper atmosphere, is given by a normalized cosine. Most of the penetrating protons are assumed to be close to the magnetic field line at the top of the atmosphere, and the field lines act as guides for the precipiting protons. Since the field lines do not converge, no back–scattering

will occur, and that is an over–simplification. The protons with small pitch-angles penetrate deeper into the atmosphere than those with large pitch-angles. Cosine pitch–angle distribution is an adequate distribution of the incoming particles, taking care of experimental facts.

In order to simplify the calculations the space is considered two dimentional, the magnetic field parallel and vertical, and the proton spectrum with the following proton aurora limited within a square plane. The density, ρ, as a function of height is obtained from the neutral atmospheric model Msis-86 (*Hedin*, 1987).

4.2 Simple method of Doppler shifted hydrogen line profiles

The geometry of emission and observing is sketched in Fig. 4.1. The hydrogen atom/proton, T, is called the transmitter, and the observer denoted by O. T is moving with kinetic energy $E(h, \theta)$ and pitch-angle θ relative to the magnetic field line $\underline{B}$. The angle between the magnetic field and the line of sight is χ.

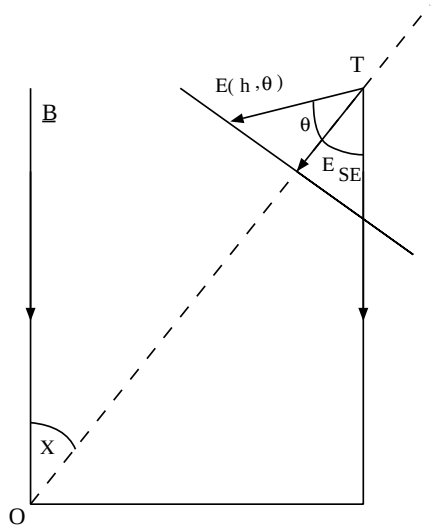

Figure 4.1: Simple configuration with vertical and parallel geomagnetic field and plane ground.

The velocity of T along the line of sight is called v_{SE}. T acts as an emitter of light with wavelength λ_0. O is at rest. To calculate the wavelength change produced by motion of the emitter in the line of sight direction, in the time $(1/\nu_0)$, where ν_0 is the frequency of the light wave, corresponding to one period of oscillation, the transmitter travels a distance $(1/\nu_0) \cdot v_{SE}$, and hence the wavelength is changed from its normal value λ_0 to a new value $\lambda = \lambda_0 \mp v_{SE}/\nu_0$ relative to O. This relation between wavelength and relative velocity occurs since the velocity is non–relativistic and the relation linear. The velocity of light is proved to be constant independent of the motion of the emitting source. Since $\nu_0 = c/\lambda_0$, O will see T emitting light with wavelength λ,

$$\lambda = \lambda_0 \cdot (1 \mp \frac{v_{SE}}{c}) \quad , where \quad v_{SE} = \sqrt{\frac{2 \cdot E_{SE}}{m_p}}, \tag{4.1}$$

when m_p is the mass of the proton. The minus sign applies to the case of T approaching O. If we know θ then the line of sight energy, E_{SE}, is given by the equation

$$E_{SE} = E(h, \theta) \cdot \cos(\chi - \theta). \tag{4.2}$$

The hydrogen atom T emits light with wavelength λ_0 and moves with the line of sight energy, E_{SE}, relative to the observer.

The instantaneous kinetic proton energy, $E(h, \theta)$, at height, h, is given by the equations (2.4) and (2.5) :

$$E(h, \theta) = E(H, \theta) - \Delta E(h, \theta),$$

where

$$\Delta E(h, \theta) = \left(\frac{1}{cos(\theta)}\right) \cdot \sum_{h=h'}^{H} \left(\frac{dE}{dR}\right) \cdot \left(\frac{\rho(h')}{\rho_0}\right) \Delta h'.$$

$E(H, \theta)$ is the initial proton energy at height H, $\Delta E(h, \theta)$ the energy loss of the proton penetrating from an upper level H down to height h (*Henriksen*, 1978). In this case H is set equal to 600 km, since the energy loss above this height is negligible. The energy degradation coefficient $(\frac{dE}{dR})$ is obtain from *Cook et al.* (1953). The initial energy $E(H, \theta)$ at the top of the atmosphere is in fact independent of θ, because the energy loss here is zero.

When the view angle χ, energy degradation, and mass density as function of height, h, are given, then the line of sight energy can be given in terms of θ and $E(H, \theta)$ at

height h, using equation (4.2) :

$$E_{SE} = \{E(H,\theta) - \left(\frac{1}{cos(\theta)}\right) \cdot \sum_{h=h'}^{H} \left(\frac{dE}{dR}\right) \cdot \left(\frac{\rho(h')}{\rho_0}\right) \Delta h'\} \cdot \cos(\chi - \theta). \qquad (4.3)$$

Thus equation (4.2) can be solved for each given $E(H,\theta)$, and find either one, two or no solutions of θ, when E_{SE} is known. These solutions will now be denoted θ_i, where $\theta_i \in [-\theta_h, +\theta_h]$ and $i \in [1,2]$. In order to explain the observed Doppler profiles the $E(h,\theta)$ components for each line of sight energy of each precipitating hydrogen atom has to be found. It is just photons with a velocity component in the line of sight direction which contribute to the Doppler profile, no one else. Fig. 4.2 shows two solutions of equation (4.3) for an initial energy of 8 keV and line of sight energy of 6 keV. The corresponding pitch–angles will be $\theta_1 = 7.8°$ and $\theta_2 = 70.3°$. In Fig. 4.3 the corresponding solutions for the given line of sight energy for more than one initial energy are shown.

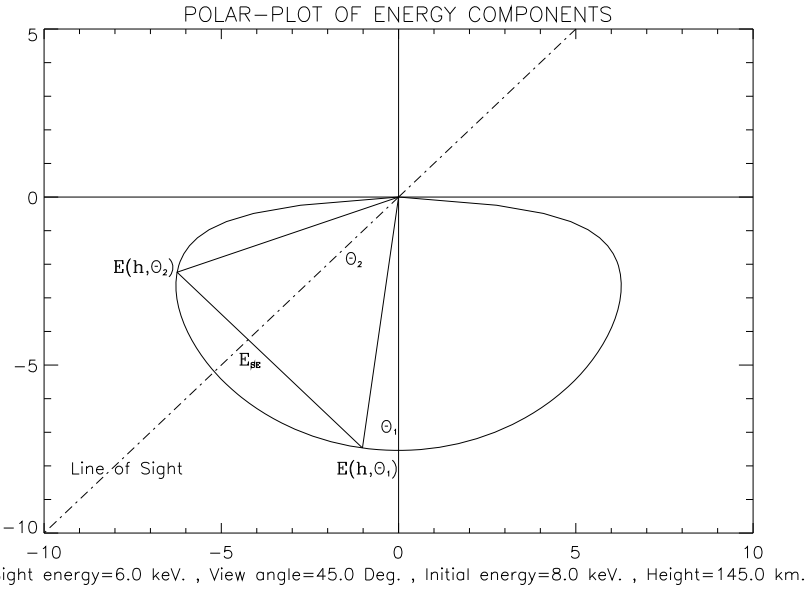

Figure 4.2: Polar plot of $E(h,\theta)$ at 145 km for given initial energy at the top of 8 keV. The sight energy is 6.0 keV and view angle 45°.

If we now know how many particles, $F(E(h,\theta_i))$, at height h that are travelling in the direction of θ_i with energy $E(h,\theta_i)$ and knows the emission rate for energetic hydrogen atoms in air, $\varepsilon_{nm}(E(h,\theta_i))$, then it is possible to calculate the total emission rate from hydrogen atoms, $\varepsilon_t(h, E(H,\theta_i))$, at height h for the given initial energy

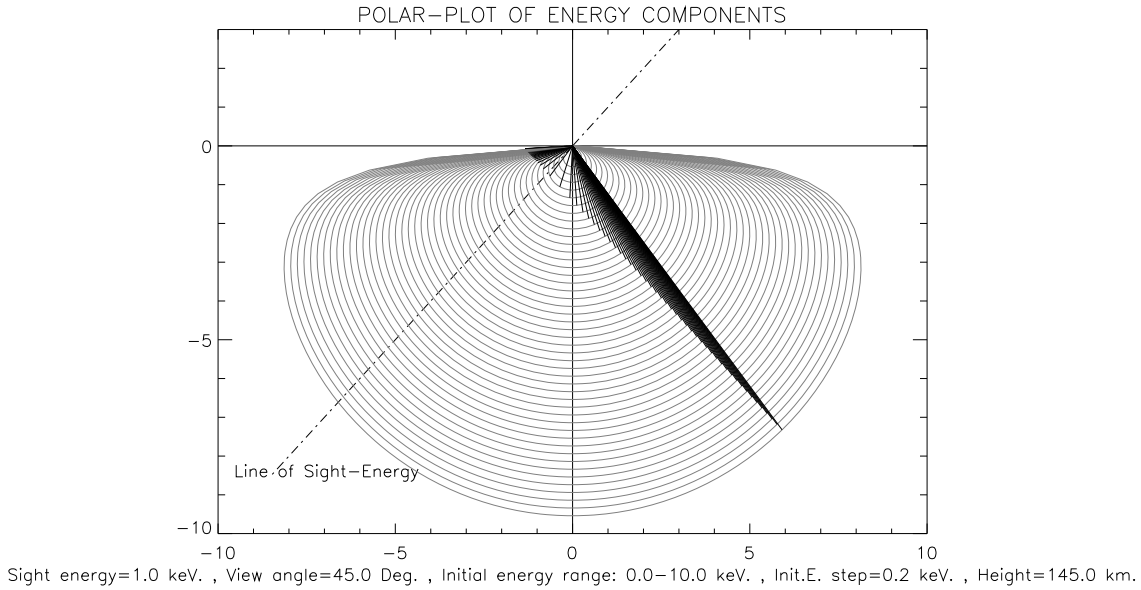

Figure 4.3: Polar plot of $E(h,\theta)$ at 145 km for variating $E(H,\theta)$. The sight energy is 1.0 keV and the view angle 45°.

and pitch–angle distribution at the top of the atmosphere by the following equations

$$F(E(h,\theta_i)) = f(E(H,\theta_i)) \cdot n(h,\theta_i),$$

$$E(h,\theta_i) = E(H,\theta_i) - \Delta E(h,\theta_i)$$

and

$$n(h,\theta_i) = \frac{1}{2} \cdot \cos\theta_i \qquad \theta_i \in [-\theta_h, +\theta_h].$$

As an example the given energy distribution at the top of the atmosphere is obtained from *Søraas et al.* (1989).

$$f(E(H,\theta_i)) = \begin{cases} 8 \cdot 10^7 \cdot E(H,\theta_i)^{-2} & E(H,\theta_i) < 100 \text{ keV} \\ 2 \cdot 10^{17} \cdot E(H,\theta_i)^{-6.67} & E(H,\theta_i) \geq 100 \text{ keV} \end{cases}$$

As previously derived equation (3.10), the emission rate for energetic hydrogen atoms travelling in the direction θ_i is :

$$\varepsilon_{nm}(E(h,\theta_i)) = \frac{A_{nm}}{\sum_{m=1}^{n-1} A_{nm}} \left(N_M \cdot \sigma_{eff}(E(h,\theta_i)) \cdot \sqrt{\frac{2 \cdot E(h,\theta_i)}{m_p}} \right).$$

The total emission rate is obtained by summing all directions :

$$\varepsilon_t(h, E(H,\theta_i)) = \sum_i F(E(h,\theta_i)) \cdot \varepsilon_{nm}(E(h,\theta_i))$$

or

$$\varepsilon_t(h, E(H, \theta_i)) = \sum_i f(E(H, \theta_i)) \cdot n(h, \theta_i) \cdot \varepsilon_{nm}(E(h, \theta_i)).$$

This expression is limited to non–relativistic kinetic energies.

The total profile, $J_\chi(h, E_{SE})$, at height h for a given line of sight energy, E_{SE}, is then simply :

$$J_\chi(h, E_{SE}) = \sum_{E(H,\theta)} \varepsilon_t(h, E(H, \theta)) \cdot \Delta E(H, \theta). \tag{4.4}$$

We now make the assumption that the area where the proton aurora occurs is limited, and that the point P has a finite extension noted as $\Delta x \cdot \Delta h$. The height ranges from 100 km to 150 km and the horizontal extent 250 km. See Fig. 4.4.

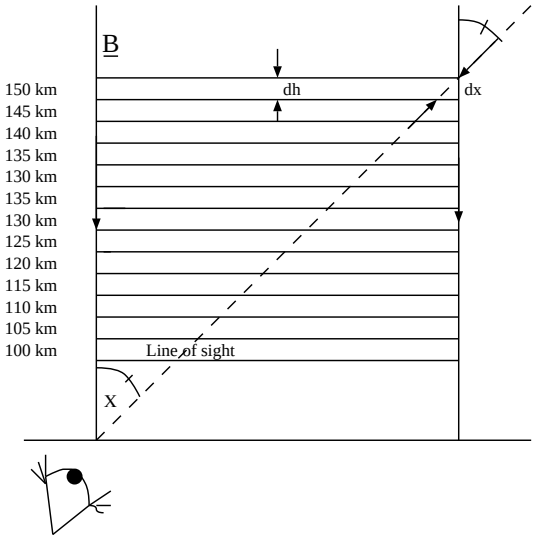

Figure 4.4: Limited aurora

The integrated profile over height, $I_\chi(E_{SE})$ for given line of sight energy E_{SE}, viewed at an angle χ to the magnetic field line, can then be calculated by adding up the contributions from each height level :

$$I_\chi(E_{SE}) = \sum_h J_\chi(h, E_{SE}) \cdot \Delta s, \tag{4.5}$$

where

$$\Delta s = \frac{\Delta h}{\cos \chi},$$

assuming a vertical and parallel magnetic field, and Δs the increment along the line of sight.

4.3 Results of modelling

Under the assumptions made in the previous sections, using the proton energy spectra from *Søraas et al.* (1989) and the normalized cosine pitch–angle distribution, we made a numerical program calculating the profile $J_\chi(h, E_{SE})$. Fig. 4.5 shows the H_α profile $I_\chi(E_{SE})$ obtained from a 5 km thick layer, ranging from 145 km to 150 km, viewed at 0°, 45° and 90° relative to the magnetic field. Since the intensity is assumed proportional with the density, then there is an intensity difference of about 5 to 250 or 1 to 50 between the zenit profile and the horizontal profile, when the width is 250 km.

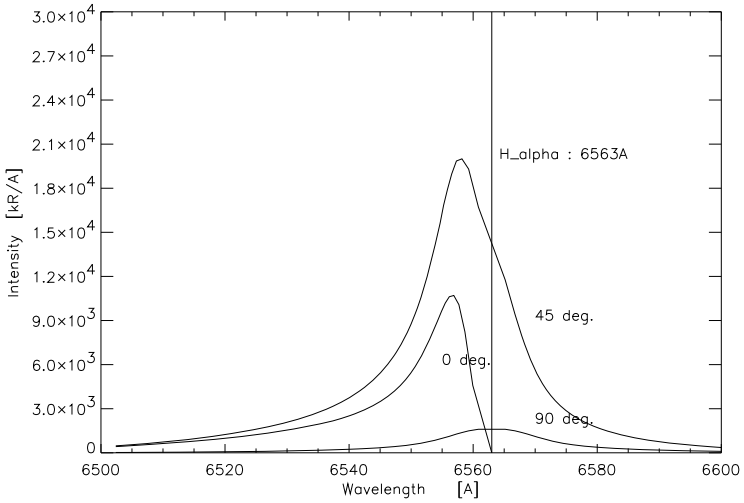

Figure 4.5: Plot of H_α from 5 km thick layer at height 145 km for three different view angles. The width of the layer is 250 km.

We can see that the horizontal profile, $\chi = 90°$, is symmetrical about $\lambda_0 = 6563\mathring{A}$, and that the zenit profile, $\chi = 0°$, has its characteristic tail shifted towards the blue part of the spectrum. We can also see that the relative intensity of the profiles increase when we turn away from zenit. This must be due to a longer optical path and more particles contribute to the emissions along this line of sight. The light at longer wavelengths than $6563\mathring{A}$ is due to particles with velocity components pointing away from the observer.

Fig. 4.6 shows the calculated H_α zenit profiles, $J_0(h, E_{SE})$, for variating heights

ranging from 100 km to 150 km.

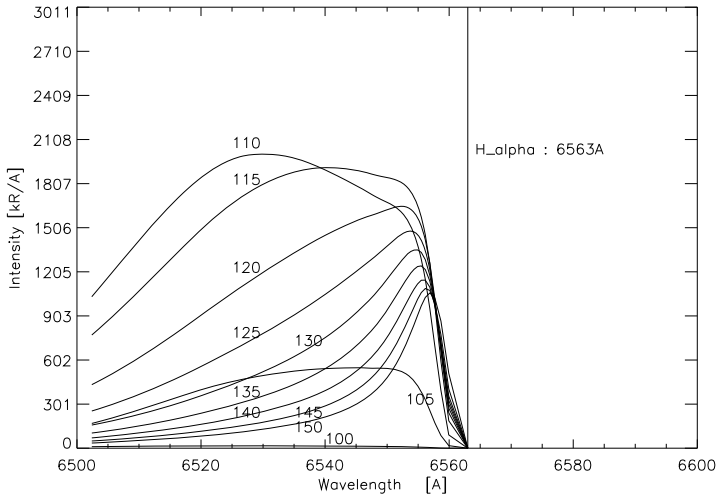

Figure 4.6: Zenit profiles for variating heights from 100 km to 150 km.

The maximum of the profiles increases and gets shifted towards the blue for decreasing height down to about 110 km. Below this height the maximum decreases quickly. The profiles also becomes wider as we go deeper down into the atmosphere. The high energetic part of the proton spectrum at the top atmosphere contributes more and more to the profiles for decreasing height. And we get more "high" energetic components contributing to the line of sight energy of the profiles.

The height integrated H_α zenit profile obtained from a 50 km thick layer, ranging from 100 to 150 km, is shown in Fig. 4.7.

The profile is wider and the tail has become more dominating than in the profile obtained in the 5 km thick layer calculation. The profile is also shifted more towards the blue. It seems like we must have a pretty soft proton spectrum at the top of the atmosphere if the observed profile is narrow.

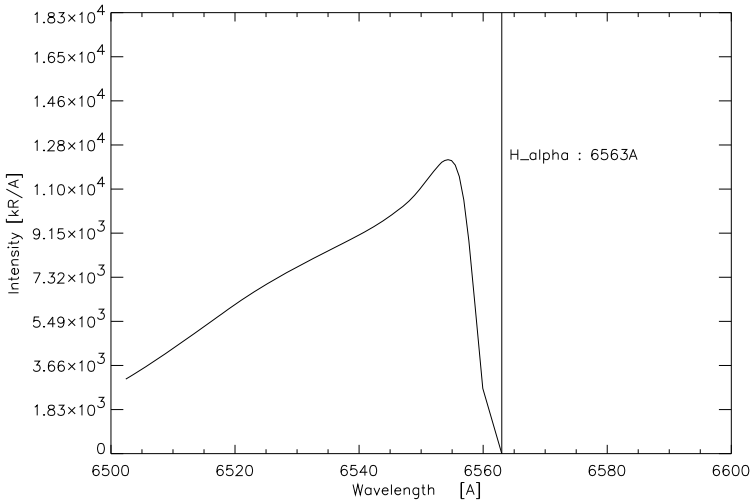

Figure 4.7: Height integrated zenit profile integrated from 100 km to 150 km.

Chapter 5

Spectrum of a diatomic molecule

We know that radiation of light in a diatomic molecule is associated with a change of dipole moment. There are two important modes of motion, namely rotation and vibration. Perturbations in these modes are the causes of emission of rotational and vibrational photons.
Calculations in this chapter are based on *Herzberg* (1967).

5.1 Synthetic spectrum of a diatomic molecule

Rotation and vibration take place simultaneously, and this combined motion of the molecule is named a vibrating rotator. The total kinetic energy of the molecule is a sum of the translational, vibrational, and rotational energies :

$$E = E_{tr} + E_v + E_r.$$

The intensity of a spectral line is dependent on the transition probability and the number of molecules in the upper energy state. At thermal equilibrium the distribution of molecules over the different possible quantum states, is normally Maxwellian.

5.1.1 Anharmonic oscillation

According to the Maxwell-Boltzmann distribution the number of molecules in the vibrational state v is :

$$N_v = \frac{N}{Q_v(T)} \cdot \exp \frac{-G(v) \cdot hc}{kT},$$

where N is the total number of molecules.
The partition function $Q_v(T)$ is given by :

$$Q_v(T) = \sum\nolimits_v \exp \frac{-G(v) \cdot hc}{kT},$$

where G(v) are called the vibrational term.

$$G(v) = \frac{E_v}{hc} \approx \omega_e \cdot (v + \frac{1}{2}) - \omega_e \chi_e \cdot (v + \frac{1}{2})^2.$$

E_v are the vibrational energy values, which again are eigenvalues of the Schrödinger equation for an anharmonic oscillator. ω_e and $\omega_e \chi_e$ are constants.

5.1.2 Non–rigid rotation

The number of molecules N_J in the rotational level J of N_v molecules is :

$$N_J = \frac{N_v}{Q_r(T)} \cdot (2J + 1) \cdot \exp \frac{-F(J) \cdot hc}{kT}.$$

The partition function of rotation is given by :

$$Q_r(T) = \sum\nolimits_J (2J + 1) \cdot \exp \frac{-F(J) \cdot hc}{kT},$$

where F(J) are called the rotational terms of a non–rigid rotator.

$$F(J) = \frac{E_r}{hc} \approx B \cdot J(J + 1) - D \cdot J^2(J + 1)^2.$$

E_r are the rotational energy values, which again are the eigenvalues of the Schrödinger equation for a non–rigid rotator, B rotational constant, and D represents the influence of the centrifugal force.

5.1.3 The vibrating rotator

So far rotation and vibration of the diatomic molecule have been regarded seperately. These two modes can take place simultaneously. Then a vibrating rotator or a rotating oscillator appears. Since the period of one vibration is small compared to the period of rotation, a mean value of the rotational constant B in the vibrational state can be used.

$$B_v \approx B_e - \alpha_e \cdot (v + \frac{1}{2}),$$

where B_e and α_e are constants. In a similar manner a mean rotational constant D_v, representing the influence of a centrifugal force, can be found.

$$D_v \approx D_e + \beta_e \cdot (v + \frac{1}{2}).$$

The rotational terms in a given vibrational level are then :

$$F_v \approx B_v \cdot J(J+1) - D_v \cdot J^2(J+1)^2.$$

The term values of the vibrating rotator are the sum of rotational and vibrational terms :

$$T = G(v) + F_v(J) \approx \omega_e \cdot (v + \frac{1}{2}) - \omega_e \chi_e \cdot (v + \frac{1}{2})^2 + B_v \cdot J(J+1) - D_v \cdot J^2(J+1)^2.$$

The wave number of a particular rotation–vibration transition from an upper state (v', J') down to a lower state (v'', J'') can now be found by :

$$\nu = F_{v'}(J') - F_{v''}(J'') + G(v') - G(v'').$$

The number of molecules in the J' rotational level of a vibrating rotator are :

$$N_{J'} = \frac{N_{v'}}{Q_r} \cdot (2J' + 1) \exp \frac{-F(J') \cdot hc}{kT},$$

where

$$N_{v'} = \frac{N}{Q'_v} \cdot \exp \frac{-G(v') \cdot hc}{kT}.$$

The number of molecules in the (v', J') state of a vibrating rotator and the intensity of the rotational emission line emitted from (v', J') to (v'', J'') is given by the relation

$$I(v', J' \rightarrow v'', J'') = N_{J'} \cdot A(v', J' \rightarrow v'', J'')$$

or

$$I(v^{'}, J^{'} \rightarrow v^{''}, J^{''}) = A(v^{'}, J^{'} \rightarrow v^{''}, J^{''}) \cdot \frac{N_{v^{'}}}{Q_r} \cdot (2J^{'} + 1) \exp \frac{-F(J^{'}) \cdot hc}{kT},$$

where $A(v^{'}, J^{'} \rightarrow v^{''}, J^{''})$ is the transition probability from state $(v^{'}, J^{'})$ to state $(v^{''}, J^{''})$ of the rotating vibrator. The transition probabilities are tabulated (*Krassovsky et al.*, 1962; *Mies*,1974), or be derived from the Schrödinger equation.

Sofar, the diatomic molecules are considered as simple rotation-vibration molecules. The OH $^2\sum M$ (6,1) - spectra observed can not be interpreted as rotation-vibration spectra alone. They are also influenced by electrons present, which give raise to two separate rotational energy terms for the doublet states (*Hill and Van Vleck*, 1923) :

$$F_v(J) = \begin{cases} B_v \cdot [(J + \frac{1}{2})^2 - 1 - \frac{1}{2}\sqrt{4(J + \frac{1}{2})^2 + Y(Y - 4)}] - D_v \cdot J^4 & ; K = J + \frac{1}{2} \\ B_v \cdot [(J + \frac{1}{2})^2 - 1 + \frac{1}{2}\sqrt{4(J + \frac{1}{2})^2 + Y(Y - 4)}] - D_v \cdot (J + 1)^4 & ; K = J - \frac{1}{2} \end{cases}.$$

More simple, if $K = J + \frac{1}{2}$ then $F_v(J) = F_1(J)$ and if $K = J - \frac{1}{2}$ then $F_v(J) = F_2(J)$. These terms can be used to make synthetic spectra of the observed OH(6,1) band. The total energy of the molecule is a sum of the electronic, vibrational and rotational energies

$$E = E_e + E_v + E_r,$$

and the correspoding wave number

$$\nu = T^{'}{}_e - T^{''}{}_e + F_v(J^{'}) - F_v(J^{''}) + G(v^{'}) - G(v^{''}),$$

which also can be expressed as

$$\nu = \nu_0 + F_v(J^{'}) - F_v(J^{''}),$$

where T_e is the electronic energy term, ν_0 the band origin, constant in each specific vibrational transition.
The relations above can be summarized to give the essence of formulas necessary to carry out calculations of the synthetic spectra for doublet rotational transitions. The internal energy of the gas in a specific electronic e, vibrational v and rotational r state is

$$E_{int} = N_e \cdot E_e + N_v \cdot E_v + N_1 \cdot F_1 \cdot hc + N_2 \cdot F_2 \cdot hc,$$

where the subscripts 1 and 2 represents the levels of a doublet.
The internal partition function is

$$Q_{int} = Q_e \cdot Q_v \cdot Q_1 \cdot Q_2,$$

where $Q_1 = \sum_{J=\frac{3}{2}}^{\infty}(2J+1)\exp\frac{-F_1(J)\cdot hc}{kT}$ and $Q_2 = \sum_{J=\frac{1}{2}}^{\infty}(2J+1)\exp\frac{-F_2(J)\cdot hc}{kT}$.
The number of molecules in the $J^{'}$ rotational level :

$$N_{J'} = \begin{cases} \frac{N}{Q_{int}} \cdot (2J^{'}+1)\exp(\frac{-F_1(J^{'})\cdot hc}{kT}) & ;K = J+\frac{1}{2} \\ \frac{N}{Q_{int}} \cdot (2J^{'}+1)\exp(\frac{-F_2(J^{'})\cdot hc}{kT}) & ;K = J-\frac{1}{2} \end{cases}.$$

The intensity of the rotational emission line emitted from $(v^{'}, J^{'})$ to $(v^{''}, J^{''})$:

$$I(v^{'}, J^{'} \rightarrow v^{''}, J^{''}) = \begin{cases} A_1(v^{'}, J^{'} \rightarrow v^{''}, J^{''}) \cdot \frac{N}{Q_{int}} \cdot (2J^{'}+1)\exp(\frac{-F_1(J^{'})\cdot hc}{kT}) & ;K = J+\frac{1}{2} \\ A_2(v^{'}, J^{'} \rightarrow v^{''}, J^{''}) \cdot \frac{N}{Q_{int}} \cdot (2J^{'}+1)\exp(\frac{-F_2(J^{'})\cdot hc}{kT}) & ;K = J-\frac{1}{2} \end{cases}, \quad (5.1)$$

where A_1 and A_2 represent the transition probabilities of molecules with positive or negative spin of the unpaired, valence electrons. The corresponding wavelengths are obtained from the expression of the wavenumber $\lambda = \frac{1}{\nu}$.

Calculations of synthetic spectra are carried out with the above expressions, and in Fig. 5.1 the synthetic OH(6,1) spectrum and a measured H_α–profile viewed at 71° relative to the magnetic field are shown. All the constants used in calculation of the intensities are from *Krassovsky et al.* (1962) and *Mies* (1974). The intensity value with corresponding wavelength is convolved with a triangular function $\Delta(\lambda)$:

$$I_{instrument}(\lambda) = I(\lambda) * \Delta(\lambda) = \sum_{k=-\infty}^{+\infty} I(\lambda - k) \cdot \Delta(k).$$

$\Delta(\lambda)$ as a baselength of two times the bandpass of the instruments. Then the halfwidth of the lines is the same as the bandpass of the instrument. The synthetic spectrum can be fitted to the measured OH(6,1)–spectrum by measuring at least two intensity values of the OH(6,1) lines outside the H_α–profile. We then have at least two equations of (5.1) for the two unknowns $\frac{N}{Q_{int}}$ and T. The resulting synthetic OH(6,1)–spectra can then be subtracted from the measured spectra and the clean H_α profile will appear.

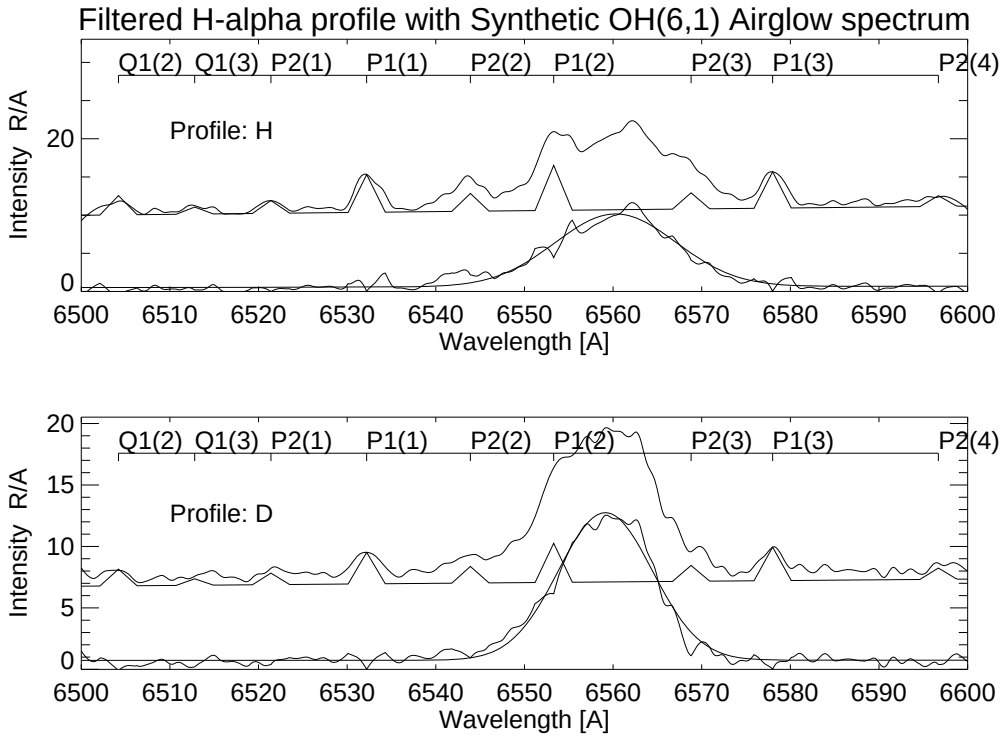

Figure 5.1: OH(6,1) synthetic spectrum calculated with bandpass equals to 2.1 Å and temperature 216 K. The above part is the synthetic and the measured spectra, and the lower part the resulting H_α profile.

Chapter 6

Instrumentation and Measurements

This chapter contains how the used instrument, an Ebert-Fastie spectrometer, is designed and works. Measurements of the hydrogen lines, H_α and H_β, are shown at the end of this chapter.

6.1 Short historical background of instrument

In 1889 Herman Ebert described a spectrometer using a spherical mirror and a plane grating (*Ebert*, 1889). His sketch is reproduced in Fig. 6.1 and shows the instrument as a photographic spectrograph. This optical system, the Ebert monochromator, was forming sharp images for a very narrow spectral range.

Later in 1952 William G. Fastie improved the preformance of the instrument, using curved slits instead of straight slits (*Fastie*, 1952). Problems of astigmatism became less, and the resolution of the instrument was improved. The instrument is now known as the Ebert-Fastie spectrometer.

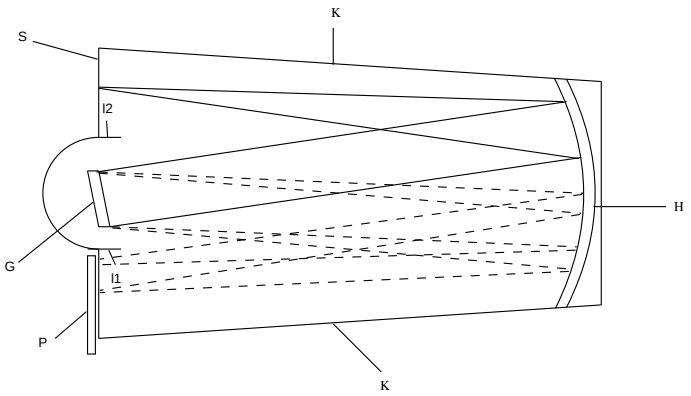

Figure 6.1: Reproduction of Ebert's sketch of his spectrometer.

6.2 Basic configuration

To explain measured data, an accurate description of the instrument, its entrance optics and use is required.

6.2.1 Experimental configuration

The observation are carried out at Nordlysstasjonen, Longyearbyen, Svalbard (78.2°N, 15.6°E; geogr. coord.). The instruments, two Ebert-Fastie spectrometers, are located inside the station. A periscope, which can be turned in different directions along the geomagnetic meridian, is the entrance optics to the spectrometers. The measurements are carried out at different angles relative to the the magnetic field lines. The field of view is 4-5 degrees.

The spectrometers have air cooled photomultiplier tubes, picking up all radiation passing the exit slits. The photomultipliers are connected to a PC through AD-converters and scalers giving the photon counts. The position of the gratings are continously changed by synchronous motors, turning cams. In addition the rotation of the cams determine the length of the wavelength scans. One digital clock gives the timing, and all the housekeeping data are provided to the computer and appear

at the beginning of each data record. (See Fig. 6.2).

The spectrometers are operated in photon-counting mode and looking in different angles relative to the magnetic field lines.

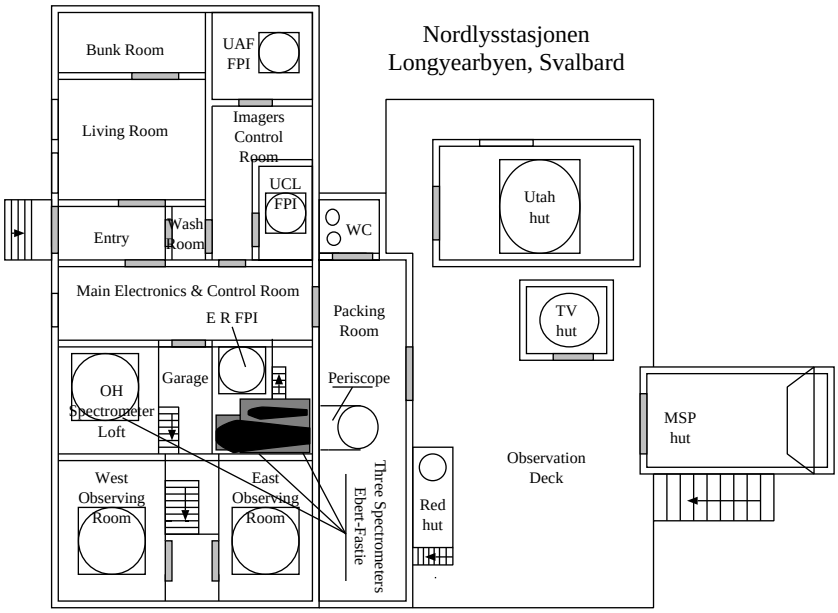

Figure 6.2: Schematics of Nordlysstasjonen and its content. The Ebert–Fastie spectrometers and their entrance optics are marked.

6.2.2 Ebert-Fastie configuration

The aim of the Ebert-Fastie spectrometer is to form a spectrum of the emissions present in an arbitrary light source, intensity for each wavelength with a certain resolution.

The instrument consists mainly of one large sperical mirror, one plain diffraction grating and a pair of slits. The light from the external source, in our case the proton aurora, is limited by the entrance slit. This entrance image is reflected and focused by the spherical mirror onto the plane grating. The mirror then focuses the diffracted light from the grating into the exit plane. When the grating turns, the image of the entrance slit is observed at the exit slit in differents wavelengths, determined by the setting of the wavelength scan. (See Fig. 6.3).

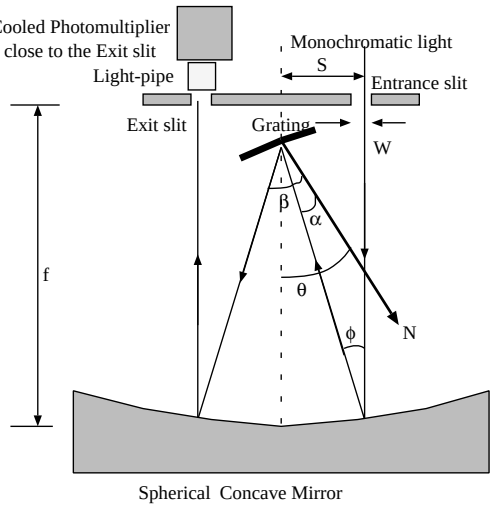

Figure 6.3: Configuration of Ebert-Fastie.

6.3 Basic calculations in use

In order to understand the work of an Ebert-Fastie spectrometer it is necessary to do some simple calculations. The performance of the instrument dependents on linear and angular dispersion, bandpass and calibration. The operation of a perfect instrument is outlined with no aberrations as misalignment, astigmatism and grating ghosts.

6.3.1 Definitions

The Ebert–Fastie spectrometer has several basic parameters, and they can be defined as :

N - grating normal.

θ - grating angle.

s - $\frac{1}{2}$ slit - slit distance.

f - focal length of the spherical mirror. The focal length is ideally $\frac{R}{2}$, where R is the radius of the concave spherical mirror.

β - diffraction angle.

α - incidence angle.

a - grating constant.

ϕ - constant for given spectrometer.

$\tan(\phi) = \frac{s}{f}$.

w - slit width.

λ - wavelength.

n - spectral order.

I - Half meter focal length Ebert-Fastie spectrometer.

II - One meter focal length Ebert-Fastie spectrometer.

The parameters are displayed in Fig. 6.3.

6.3.2 Angular dispersion

The most fundamental equation for a spectrometer is the grating equation :

$$n \cdot \lambda = a\,(\sin\alpha + \sin\beta)\,. \tag{6.1}$$

The parameters are visualized in Fig. 6.4.

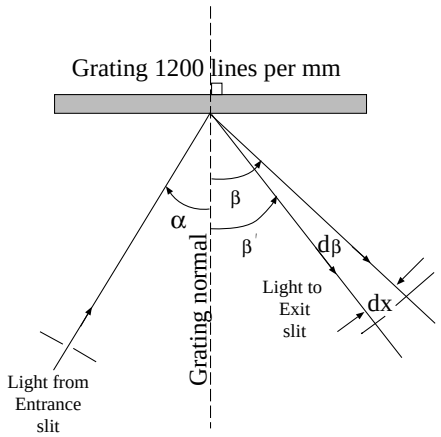

Figure 6.4: Parameters of grating equation.

The grating equation can be transformed, $\alpha = \theta - \phi$ and $\beta = \theta + \phi$, then

$$n \cdot \lambda = a \cdot (\sin\theta \cdot \cos\phi - \sin\phi \cdot \cos\theta + \sin\theta \cdot \cos\phi + \sin\phi \cdot \cos\theta)$$

and

$$n \cdot \lambda = 2 \cdot a \cdot \sin\theta \cdot \cos\phi.$$

Then $\frac{d}{d\beta}(n \cdot \lambda)$ simply becomes :

$$\frac{d}{d\beta}(n \cdot \lambda) = a \cdot \cos\beta, \tag{6.2}$$

where $d\beta$ is the angular separation between two emissions and $d\lambda$ the wavelength separation between two emissions. Angular dispersion is then defined as :

$$\frac{d\lambda}{d\beta} = (\frac{a \cdot \cos\beta}{n}).$$

6.3.3 Linear dispersion

When $d\beta$ is small, the corresponding distance in the exit plane will be $dx = f \cdot d\beta$. Then the linear dispersion, $\frac{d\lambda}{dx}$, is given by :

$$\frac{d\lambda}{dx} = \frac{d\lambda}{f \cdot d\beta} = \frac{a \cdot \cos\beta}{n \cdot f},$$

where f is the focal length of the mirror. Linear dispersion defines the extent to which a spectral interval is spread out across the focal field of the spectrometer. So, linear dispersion is associated with the instruments ability to resolve fine spectral detail.
Since $\beta = \theta + \phi$,

$$\frac{d\lambda}{dx} = \frac{a \cdot \cos(\theta + \phi)}{n \cdot f}. \tag{6.3}$$

We can see from equation (6.3) that the linear dispersion becomes smaller for higher spectral order. However, in order to get greater resolution higher spectral orders are used, but then normally the throughput decreases. A filter in front of the entrance slit is normally used to prevent overlapping orders. Throughput, the usable photon flux at the exit slit, is influenced by the order-sorting filter, because the filter itself has a characteristic transmission response dependent on wavelength. Normally compromise has to be made between ability of the instrument to resolve spectral details and expected throughtput. The result of the compromise can be studied by absolute intensity and wavelength calibration.

6.3.4 Bandpass

The bandpass of the instrument can now be found by multiplying the width of the exit slit with the linear dispersion :

$$BP = \frac{d\lambda}{dx} \cdot w, \tag{6.4}$$

Normally the entrance and exit slits have the same width. Then BP is the instrumental line width, the half–width of a inifinite narrow line passing through the instrument and recorded. By half–width is meant the width at half of the intensity maximum. When the entrance and the exit slits are equal, straight, and parallell, the profile of the line will be triangular, and similar for perfectly matched curved slits.

6.4 Calibration of instrument

The desired spectral range of the instrument can be controlled by wavelength calibration, and the intensities measured by the instrument obtained by comparison with a well known light source. For quantative, spectral measurements it is absolutely necessary that the instrument is calibrated both for wavelength and intensity. Calibration procedures will be outlined below.

6.4.1 Absolute calibration

There is always loss of light, photons, when the light passes through the instrument and the photons being transformed to electronic pulses by the photomultiplier. The throughput can be considered as an equivalent for the sensitivity or wavelength dependent calibration curve of the instrument, giving the ratio of electronic counts out to the number of photons hitting the instrument. It is necessary to calibrate the instrument against a known light source to obtain the spectrum in absolute units. Our absolute calibration configuration is sketched in Fig. 6.5.

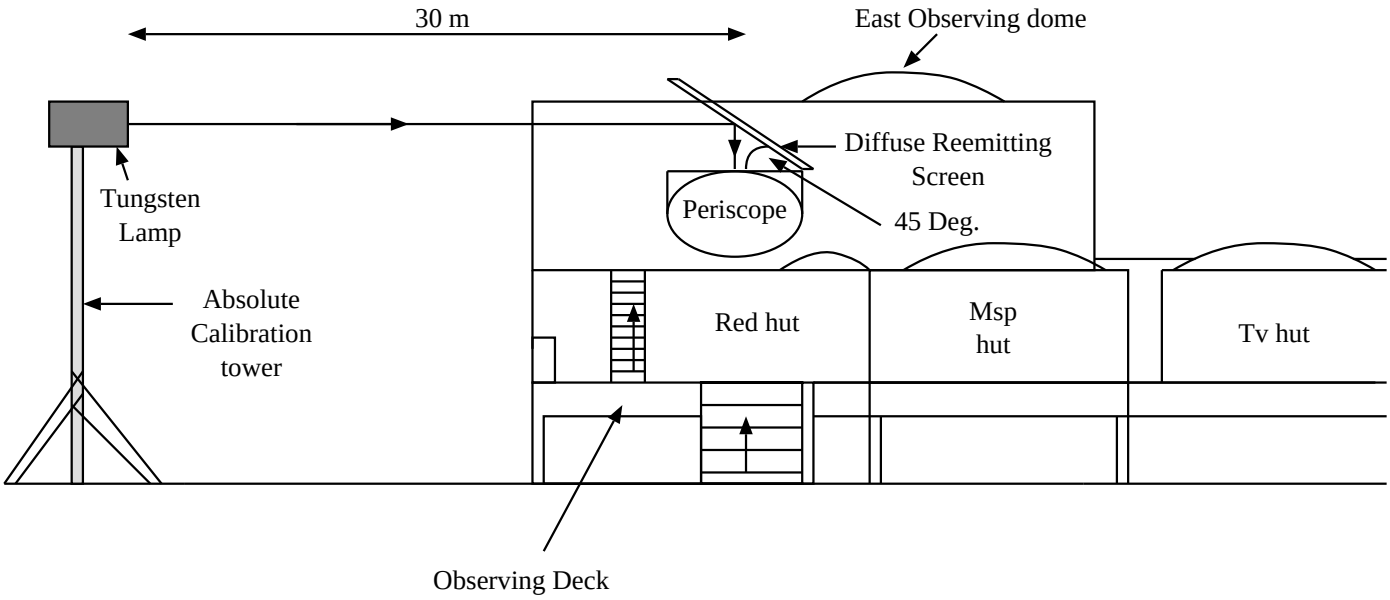

Figure 6.5: Configuration of the setup for absolute calibration.

The field of view of the instrument has to be inside the fully illuminated area of the screen, which is diffuse by reemitting. $B_0(\lambda)$ is the known intensity of the Tungsten lamp in Rayleigh per Ångstrøm, obtained at a distance r away from the lamp. The intensity $B(\lambda)$ of the screen at a distance R away from the lamp would then be:

$$B(\lambda) = B_0(\lambda) \cdot \left(\frac{r}{R}\right)^2 \cdot \cos\Psi \qquad [\frac{R}{\mathring{A}}].$$

$C(\lambda)$ is the counts per unit time produced by the intensity of the Tungsten lamp. The calibration factor $K(\lambda)$ is then :

$$K(\lambda) = \frac{B(\lambda)}{C(\lambda)} \qquad [\frac{R}{\mathring{A}(counts/sec)}] \tag{6.5}$$

or

$$K(\lambda) = \frac{B_0(\lambda)}{C(\lambda)} \cdot \left(\frac{r}{R}\right)^2 \cdot \cos\Psi.$$

A measured hydrogen line profile with relative intensity $I_N(\lambda)$, counts per unit time, will then have the intensity $I(\lambda)$ in absolute units :

$$I(\lambda) = K(\lambda) \cdot I_N(\lambda) \qquad [\frac{R}{\mathring{A}}]. \tag{6.6}$$

$C(\lambda)$ and $I_N(\lambda)$ must be measured in the same units, using the same time unit. The total intensity of the profile would then be :

$$I_T = \int_{\lambda_1}^{\lambda_2} I(\lambda) d\lambda, \tag{6.7}$$

where λ_1 and λ_2 respectively represent lower and upper limits of the profile.

6.4.2 Wavelength calibration

In order to calibrate the spectrum in wavelength specific line emission lamps with known spectral lines have to be used. The emitting gas of these lamps are Argon, Krypton, Helium, Neon, Xenon and Mercury. It is, depending on wavelength region of interest, needed at least two known lines within the region to adjust the scale. When λ_1 and λ_2, $\lambda_2 > \lambda_1$, are the known lines inside the wavelength region of interest, an arbitrary wavelength λ can then be found by the simple relation

$$\frac{\Delta z}{\Delta z_0} = \frac{(\lambda_2 - \lambda_1)}{(\lambda_2 - \lambda)}, \tag{6.8}$$

where Δz is the distane between λ_2 and λ_1, and Δz_0 the difference between λ and λ_2. Eq. (6.8) can only be used when the wavelength drive is sufficiently linear.

6.4.3 Instrumental parameters

The basic instrument parameters due to the simple calulations done in section (6.3) are presented in Table (6.1). The bandpass, $BP = \frac{d\lambda}{dx} \cdot w$, of spectrometer I and

Spectrometer focal length f (m)	*Wavelength region (Ångstrøm)*	*Spectral order n*	*Filter color*	*Linear dispersion (Ångstrøm/mm)*	*Slit width (mm)*
I: 0.5	6331-6667	2	yellow	4.2	0.5
II: 1.0	4785-4873	3	blue-green	1.0	1.0

Table 6.1: Instrumental parameters.

II is then respectively 2.1 and 1.0 Ångstrøm. The functions needed in absolute calibration, see equation (6.5), are fitted to obtain a calibration factor, $K(\lambda)$, for each wavelength region of interest.
The following are obtained :

$$R \approx 30.0m, \quad r \approx 8.4m, \quad \textit{and} \quad \Psi \approx 45^\circ.$$

The known intensity of the Tungsten lamp can be approximated by the following equation

$$B_0(\lambda) \approx 34165.3 - 22.4 \cdot \lambda + 0.004 \cdot \lambda^2 - 2.2 \cdot 10^{-7} \cdot \lambda^3 \qquad [\frac{R}{\mathring{A}}]$$

and

$$B(\lambda) \approx B_0(\lambda) \cdot (\frac{8.4}{30.0})^2 \cdot \cos 45^\circ \qquad [\frac{R}{\mathring{A}}].$$

The measured relative intensity of the Tungsten lamp is

$$C_I(\lambda) \approx \lambda - 4410.0 \qquad [\frac{counts}{sec}]$$

and

$$C_{II}(\lambda) \approx -0.09 \cdot \lambda + 584.3 \qquad [\frac{counts}{sec}].$$

The calibration factors for spectrometer I and II are then respectively $K_I(\lambda) \approx \frac{B(\lambda)}{C_I(\lambda)}$ and $K_{II}(\lambda) \approx \frac{B(\lambda)}{C_{II}(\lambda)}$.

6.5 Measurements of the hydrogen line profiles

A small change in the view angle of the instruments will lead to a change in shape of the of the hydrogen line profiles. Measuring the hydrogen line profiles, a vertical and parallel magnetic field line was assumed. This is not the case, because the magnetic field deviate from the vertical at the observation site. Therefore the magnetic field line configuration at the observational site has to be calculated to get the right view angle realtive to the magnetic field.

The proton events of interest occurred on the 22th and the 23th of January 1991. Between 00.00 and 07.00 UT hydrogen profiles were observed at arbitrary angles to the magnetic field lines. To get a general view of the proton events, data from other instruments than the spectrometers will also be presented.

6.5.1 The magnetic field

The earth's magnetic field in the upper atmosphere is very simular to the field of a dipole located near the center of the earth. Hence, one usually express the properties of the main field in terms of this centered dipole approximation, by means of "dipole" or "geomagnetic" coordinates. The dipole field can be expressed in a radial and a tangential component

$$B_r = -2 \cdot \sin \wedge R^{-3} \cdot B_{eq} \tag{6.9}$$

and

$$B_\lambda = \cos \wedge R^{-3} \cdot B_{eq},$$

where B_{eq} is the avarage value of $\underline{B}$ at the geomagnetic equator equal to $31 \cdot 10^{-6}$ T and $\wedge$ the geomagnetic latitude equal to 73.1° at the observational site in Svalbard. The radial distance R is measured in terrestrial radii :

$$R = \frac{z + R_0}{R_0},$$

where R_0 is the radii of the earth and z the altitude.
These expressions are obtained from *Giraud and Petit* (1978). The radial component is directed downward, and has a minus sign in the northern hemisphere. The tagential component is directed nortward in both hemispheres. Using these expressions the downward angle of inclination, I, of the magnetic field line vector, $\underline{B}$, from the horizontal plane is :

$$I = arctan(-\frac{B_r}{B_\lambda}). \tag{6.10}$$

From the equations (6.9) and (6.10) we then get :

$$I = arctan(2 \cdot tan \wedge), \tag{6.11}$$

which gives us a dip angle at the observational site to be $I \approx 81.36°$.

It is possible to calculate the dip angle as a function of height from the magnetic field line model IGRF (*Barraclough*, 1987). This model is a good approximation of the magnetic field out to about five earth radii, assuming that the Earth's magnetic field can be derived from a potential which satisfies the Laplace equation. The output of this model is the X,Y and Z components of the magnetic field vector $\underline{B}$ as a function

of height at the desired location in geographic coordinates and time. X and Y is in the horizontal plane, and Z is pointing towards the center of the earth, the vertical component.

The dip angle I as a function of height h in Longyearbyen can then be found by :

$$I(h) = arctan(\frac{Z(h)}{(X(h)^2 + Y(h)^2)^{\frac{1}{2}}}) \tag{6.12}$$

Fig. 6.6 shows that the dip angle as a function of height is almost constant (*T. Sparr, private communication*, 1991). This is not far from the value obtained by assuming the magnetic field to be similar to the field of a dipole.

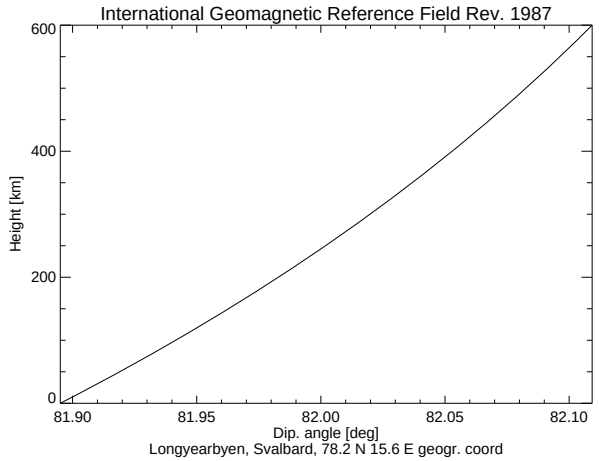

Figure 6.6: Dip angle as a function of height in Svalbard.

Then the magnetic field up to 600 km is nearly parallel and straight with a dip angle of about 82°. The magnetic zenit at the observational site is then directed southward 8° off the vertical. Due to these calculations, our view angles where 19°, 26° and 71° to the magnetic field lines.

A magnetometer in Ny-Ålesund, Svalbard ($78.9°N, 11.9°E$; geogr. coord.) shows the components of the magnetic field at ground level for the 22th and the 23th of January 1991 (*B. Holmslett, private communication*, 1991). (See Fig. 6.7 and 6.8).

The horizontal component H, the vertical component Z and the declination D of the total field $\underline{B}$ only deviated a few prosents off the baseline values, and in absolute unit the mean magnetic deviation of these events equals to about 100 γ. So, the geomagnetic activity was low during the proton events, and the proton precipitation did not generate strong ionospheric currents.

Figure 6.7: The components of the magnetic field at ground level for the 22th of January 1991, Svalbard

6.5.2 The meridian scanning photometer

A five channel meridian scanning photometer, the MSP, measured the intensities at the wavelengths 6300Å, 5577Å, 4861Å, 5200Å and 7320Å. Unfortunately two of the channels, the channels measuring at the wavelengths 4861Å and 7320Å, where not operating properly.

Fig. 6.9 and 6.10 show plots of the 6300Å, the 5577Å and the 5200Å emission line intensities as a function view angle and time (*J. Minow, private communication*, 1991). The plots are of the average of 60 scans, or 15 minutes, plotted at the startpoint in time. That is, a value for 06:15 UT would include data from 15 minutes after. The data are not calibrated, but are plotted in a relative scale of 1.0 : 2.06 : 0.0035 for 6300Å : 5577Å : 5200Å.

The intensities of these lines represent the activity of the electron aurora, aurora produced by showers of incoming electrons shot into the atmosphere. The red line 6300Å and the green line 5577Å are forbidden atomic oxygen lines, while the 5200Å line is a forbidden atomic nitrogen doublet. However, some unknown contributions to these line emissions may have been generated by the concurrent proton influx.

Figure 6.8: The components of the magnetic field at ground level for the 23th of January 1991, Svalbard

The activity was low both nights. It seemed like the activity was moving south-northwards, starting in the south at about 00:00 UT and moving slowly towards north. And at about 04:00 UT the activity was in the north. It seems like we turned the periscope of the spectrometers in the direction of this activity, but it was not the intention. (See table 6.2). It may just be that we have weak electron aurora present at the same time and place as the proton aurora.

6.5.3 The spectrometers

Throughout these clear moonless nights, the 22th and the 23th of January 1991, the H_β and H_α hydrogen line profiles where measured at the view angles of 71°, 26° and 19° relative to the magnetic field. Table (6.2) describe the position of the periscope in degrees χ_p, or the view angle χ_m of the instruments relative to the magnetic field. When the periscope is directed towards the southern horizon, then it is in the $\chi_p = 0°$ position.

The table (6.2) also indicate the motion of the proton events. The proton aurora seemed to move in the south-north direction. We started to measure at an angle

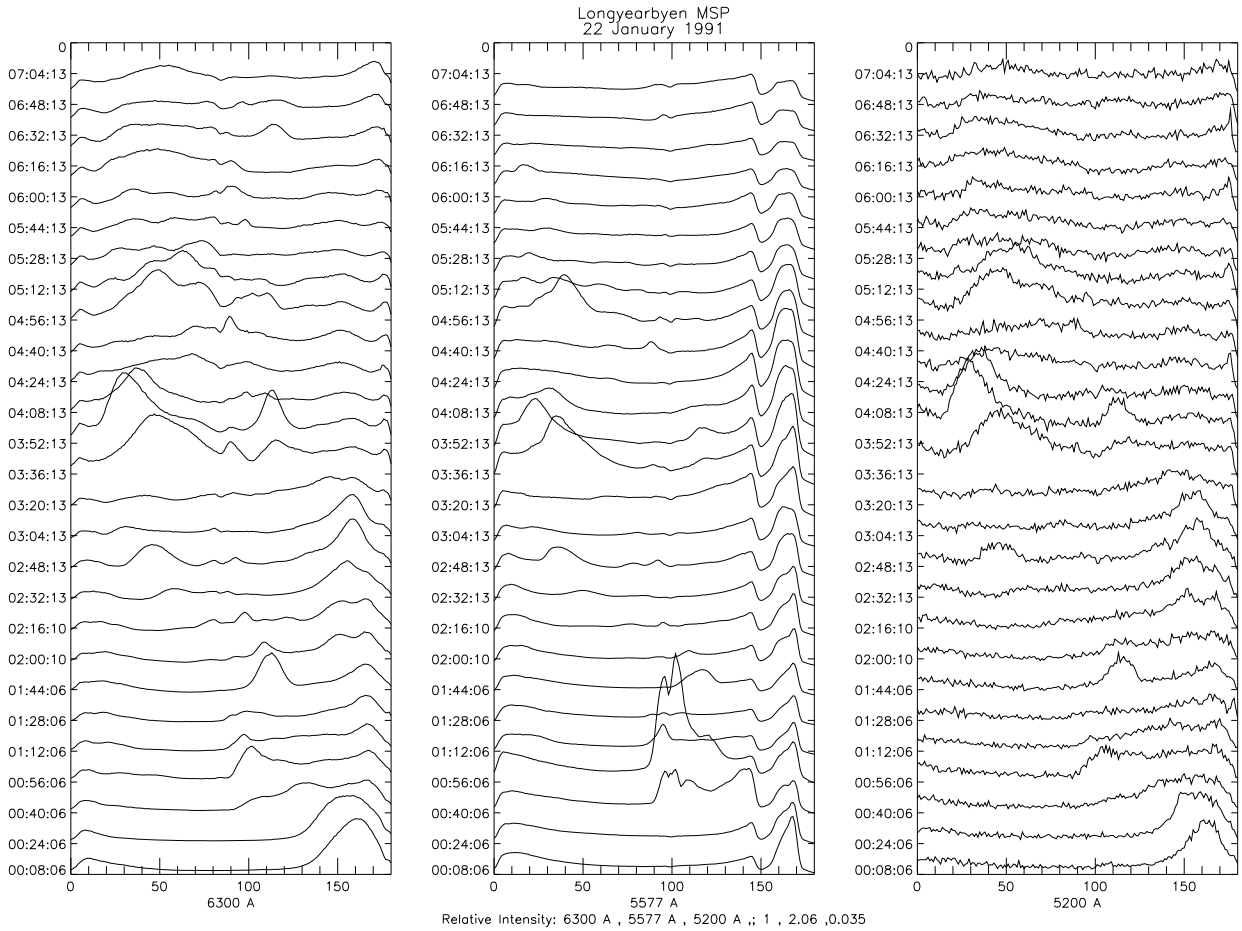

Figure 6.9: MSP data for the 22th of January 1991

of 71° relative to the magnetic field, which was in our case looking south 169° with the periscope. After this period of three hours we tried to look in the direction of 19° relative to the magnetic field, but we could not see any hydrogen profiles. It seemed like the activity was moving northwards, and we respectively measured profiles in about one and two hours at the view angles of 26° and 19° relative to the magnetic field. Then we turned the periscope back to the first position, but could no see any activity. We ended up looking 11° off the vertical directed northwards. We turned off the spectrometers when we recognized the Fraunhofer lines of H_α and H_β, indicating influence of direct sunlight, caused by absorption of the corresponding wavelengths from the hotter regions of the Sun. The Fraunhofer line starts to grow when the local solar depression angle is less than approximately 13° and makes the correspondig H_β emission very hard to measure (*Henriksen et al.*, 1985). The next night, the 23th of January 1991, the procedure was repeated, and we managed to

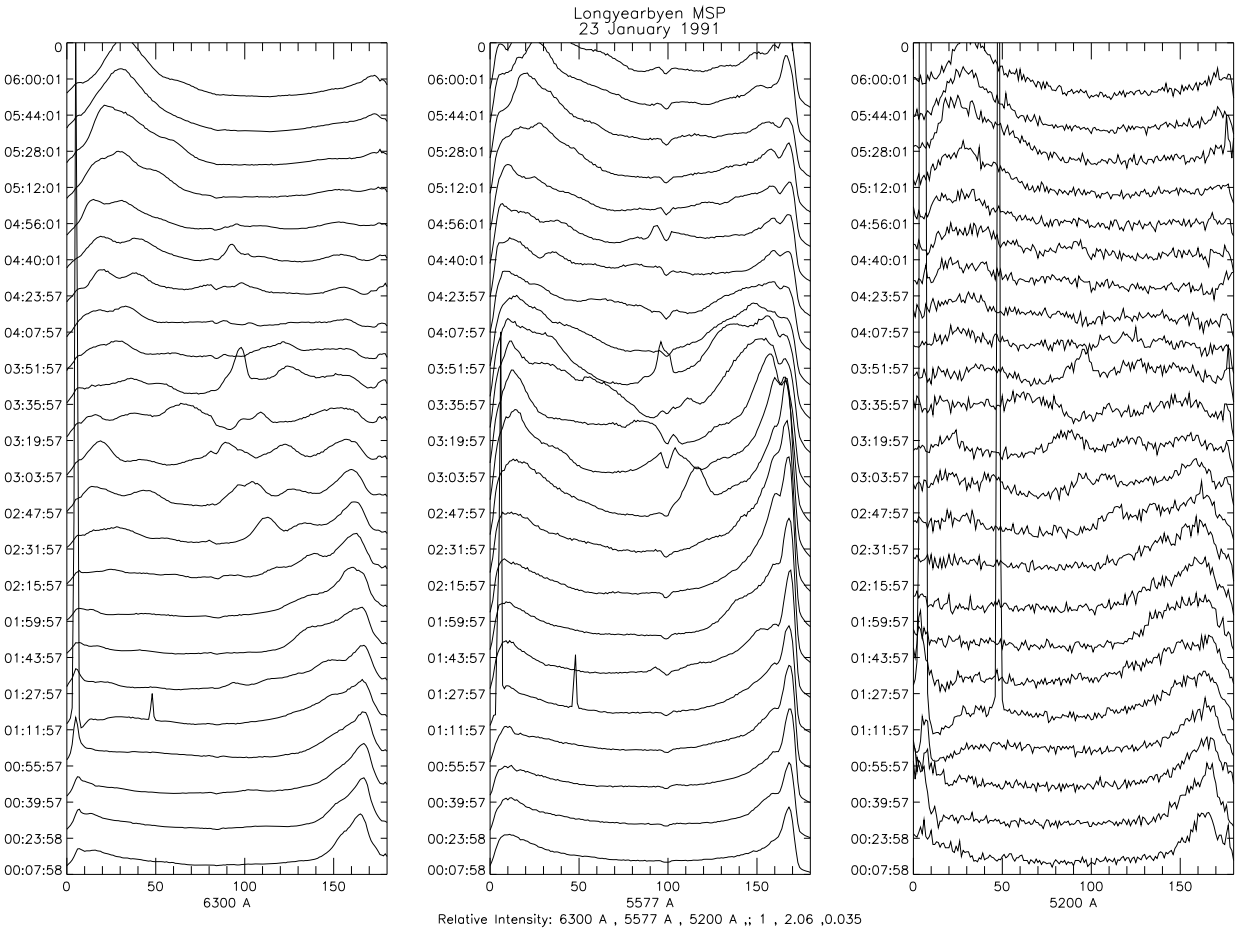

Figure 6.10: MSP data for the 23th of January 1991

get some more data.

Each scan of spectrometer I took 12 seconds, while spectrometer II used 16 seconds. The profiles shown are averaged over the time interval of interest. It should be noted that there are lines from air–glow OH(6,1) present in the nearby H_α. These rotational lines can contribute to the H_α profile. Fig. 5.1 shows the influence of the OH(6,1) in the spectrum of the H_α profile viewed at an angle 71° relative to the magnetic field. It seemed like the OH was getting very weak when we turned towards zenit, and this can be due to the van Rhijn effect (*van Rhijn*, 1921). Looking in the horizontal direction light is collected from a thicker atmospheric layer compared with a zenit direction of view.

Date *dd:mm:yy*	*Start time* *hr:min UT*	*End time* *hr:min UT*	χ_m *degrees*	χ_p *degrees*	*Inst. I* *No. scans*	*Inst. II* *No. scans*	*Profile* *Index*
22.01.91	00:09	03:09	71	169	880	600	$\mathcal{H}$
	03:10	03:13	19	79	-	-	-
	03:14	04:13	26	124	300	210	$\mathcal{Y}$
	04:14	06:16	19	79	620	430	$\mathcal{D}$
	06:17	06:20	71	169	-	-	-
	06:21	07:00	19	79	200	110	$\mathcal{R}$
23.01.91	02:19	02:21	19	79	10	-	$\mathcal{O}$
	02:22	03:26	71	169	320	200	$\mathcal{G}$
	03:27	04:56	26	124	450	290	$\mathcal{E}$
	04:57	06:30	19	79	470	-	$\mathcal{N}$

Table 6.2: Time schedule of periscope

Fitting the measured profiles by the function :

$$I(\lambda) \approx a_0 \cdot exp^{-(\frac{(\lambda - a_1)^2}{2 \cdot a_2})} + a_3 + a_4 \cdot \lambda + a_5 \cdot \lambda^2, \tag{6.13}$$

where a_0 is the height of exp, a_1 the center of exp, a_2 the (1/e)-width, a_3 the constant term, a_4 the linear term and a_5 the quadratic term. The fitted functions with the measured profiles are shown in Fig. (6.12) and (6.11). The parameters a_0, a_1, a_2, a_3, a_4 and a_5 are given in Table (6.3) for each fitted profile.

The best data was obtained during the first night. The intensities, especially in the H_β measurements, were very low during the second night, and we were not able to see any differences in the profiles measured at the different view angles. However, the H_α measurements showed clearly distinguished profiles for each view angle at both nights. Looking at the first night, the profile $\mathcal{H}$, measured at the view angle 71° relative to the magnetic field, is broader than the profiles $\mathcal{Y}$ and $\mathcal{D}$ measured at respectively 26° and 19° relative to the magnetic field. (See Table 6.3). The $\mathcal{H}$ profile is also almost symmetrical about $\lambda_0 = 6563\mathring{A}$, while the $\mathcal{Y}$ and $\mathcal{D}$ profiles are more shifted towars shorter wavelengths. The H_β measurements show a similar behaviour for the first night, while the $\mathcal{H}$ profile is more wider and symmetrical about $\lambda_0 = 4861\mathring{A}$ than the $\mathcal{Y}$ and $\mathcal{D}$ profiles. So, it seems like the profiles, $\mathcal{H}$, $\mathcal{Y}$, $\mathcal{D}$ and $\mathcal{R}$, obtained the first night are the measurements that coincide with expectations. These profiles will in the next chapter be compared with the ones obtained from modelling. It should be noted that we had some problems with calibration of the

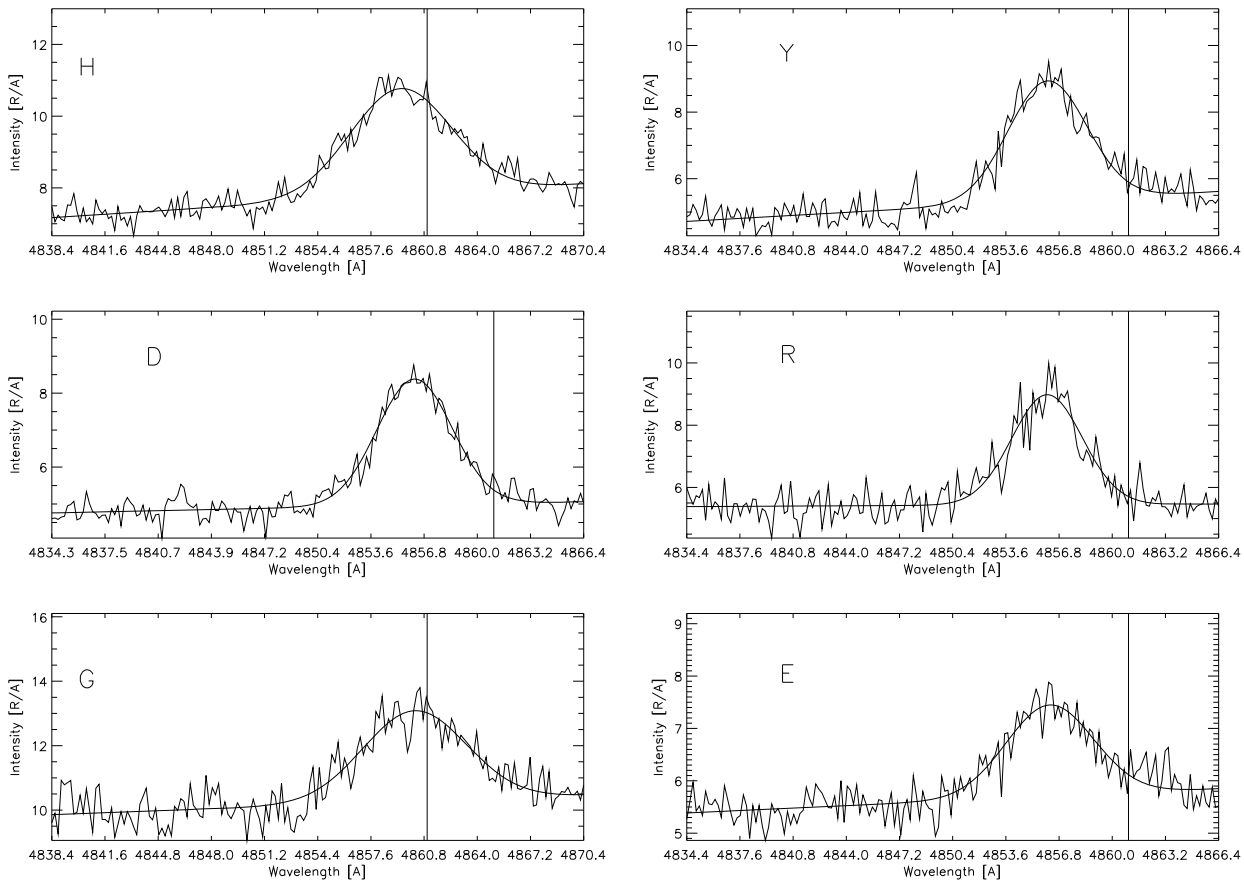

Figure 6.11: Spectrometer II : Measured H_β profiles with fitted functions.

H_β profiles. They seem to be 5 or 2 $\mathring{A}$ shifted towards higher wavelengths. And when we did absolute calibration, we got a sudden decrease of counts in the middle of the spectrum. It is most possible due to an instrumental fault, and they should not be trusted.

Since we measured H_α and H_β simultaneously, it is no doubt that these measurements are of proton aurora. The weak geocoronal hydrogen line consists only of H_α, and therefore simultaneously H_β measurements indicate the presents of proton aurora. Additionally, geocoronal H_α must be centered around $6563\mathring{A}$, appearing as a narrow line broadened by the instrumental slit function. Since there is no reason to believe that the exospheric hydrogen has a bulk motion relative to the Earth, the geocoronal H_α has to be centered around $6563\mathring{A}$. The Doppler broadening of the H_α line can be calculated by the formulas of *Chamberlain* (1961), using 2000–3000K

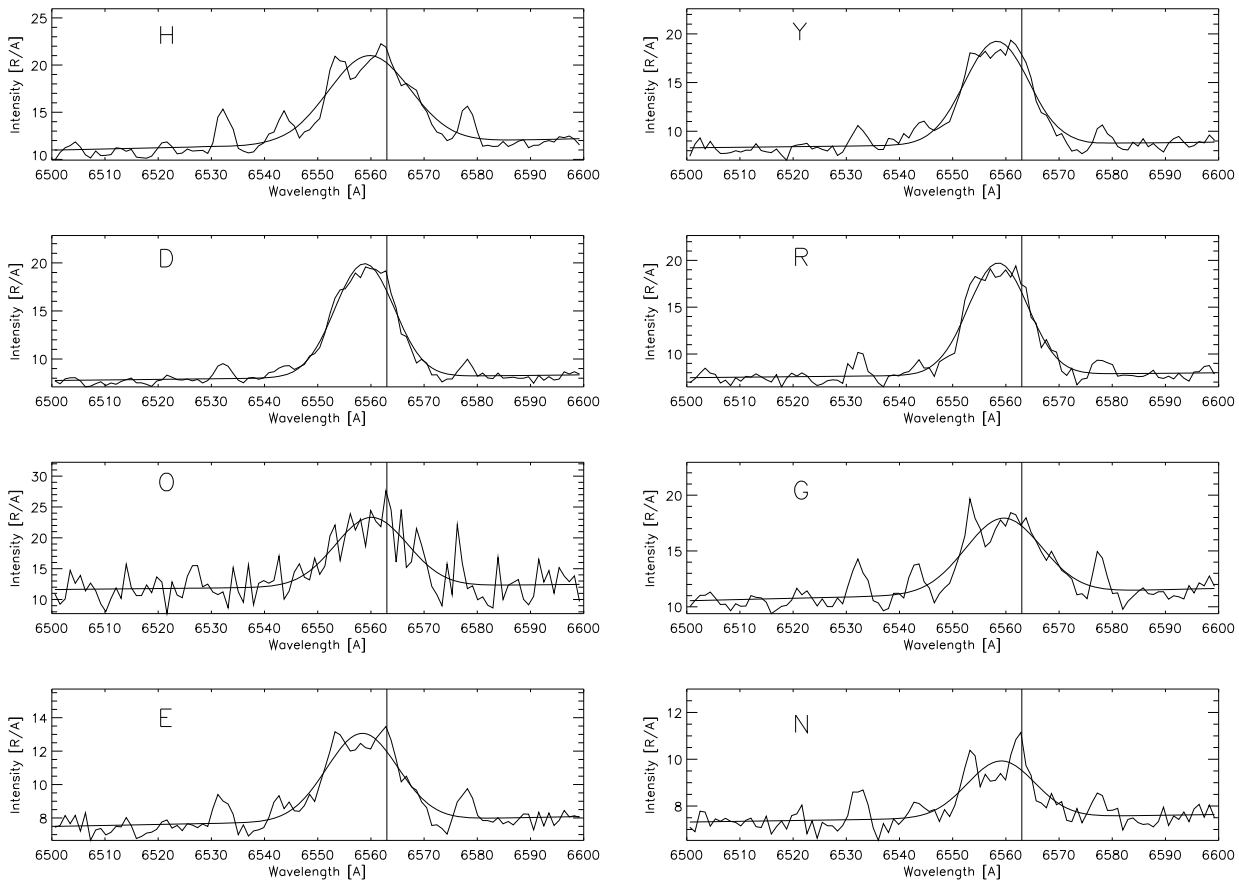

Figure 6.12: Spectrometer I : Measured H_α profiles with fitted functions.

as the exospheric temperature.

H_α	a_0	a_1	a_2	a_3	a_4	a_5	Tot. int.
Index	$R/\mathring{A}$	$\mathring{A}$	$\mathring{A}$	$R/\mathring{A}$	$R/\mathring{A}^2$	$R/\mathring{A}^3$	R
$\mathcal{H}$	9.3	6559.7	7.7	-139.4	0.03	-1.7E-06	278.5
$\mathcal{Y}$	10.6	6558.3	6.0	-84.2	0.02	-1.3E-06	259.1
$\mathcal{D}$	11.8	6558.8	5.6	-90.3	0.02	-1.4E-06	263.5
$\mathcal{R}$	11.9	6558.6	5.6	-84.3	0.02	-1.3E-06	267.2
$\mathcal{O}$	11.2	6560.1	6.8	-121.2	0.03	-1.8E-06	291.5
$\mathcal{G}$	6.7	6559.5	7.2	-110.9	0.03	-1.5E-06	220.3
$\mathcal{E}$	5.2	6558.3	6.9	-60.7	0.01	-6.9E-07	186.2
$\mathcal{N}$	2.4	6559.1	6.3	-28.7	0.01	-3.5E-07	137.3
H_β	a_0	a_1	a_2	a_3	a_4	a_5	Tot. int.
Index	$R/\mathring{A}$	$\mathring{A}$	$\mathring{A}$	$R/\mathring{A}$	$R/\mathring{A}^2$	$R/\mathring{A}^3$	R
$\mathcal{H}$	2.9	4859.4	3.1	-245.9	0.08	-4.7E-06	22.8
$\mathcal{Y}$	3.6	4856.1	2.4	-236.2	0.07	-4.5E-06	21.4
$\mathcal{D}$	3.4	4856.1	2.3	-166.5	0.06	-5.3E-06	19.4
$\mathcal{R}$	3.5	4856.1	2.1	-96.7	0.04	-3.8E-06	18.8
$\mathcal{G}$	2.8	4860.2	3.1	-187.6	0.06	-4.5E-06	21.9
$\mathcal{E}$	1.7	4856.2	2.6	-120.6	0.04	-2.4E-06	11.6

Table 6.3: Parameters to fitted profiles.

Chapter 7

Comparison between model and measurements

This chapter contains a short comparison between the simple method of calculating Doppler shifted and broadened hydrogen line profiles developed in chapter 4 and the measured hydrogen line profiles presented in chapter 6.

7.1 Measurements used to compare with modelled results

As pointed out in the previous chapter the measured profiles obtained the first night are the ones that will be used in comparing with the modelled profiles.

Since the profiles were measured at the view angles of 71°, 26°, and 19° relative to the magnetic field, the profiles at 71° and 19°, the profiles $\mathcal{H}$ and $\mathcal{D}$, will be used to compare with the modelled profiles, because the profiles measured and modelled at the view angles of 26° and 19° are too close in shape and peak intensity to give significant different results. The OH(6,1)–lines influence on the H_α profile, as pointed out in chapter 5, their contribution are evaluated and removed, and the resulting profile is compared with the modelled profile.

Fig. 7.1 shows the evaluated H_α profiles when the OH(6,1) contribution is removed by the procedure outlined in chapter 5. The resulting profiles are fitted by the function

$$I(\lambda) \approx a_0 \cdot exp^{-(\frac{(\lambda - a_1)^2}{2 \cdot a_2})} + a_3 + a_4 \cdot \lambda + a_5 \cdot \lambda^2.$$

The parameters a_0, a_1, a_2, a_3, a_4 and a_5 are given in Table (7.1) for each fitted profile.

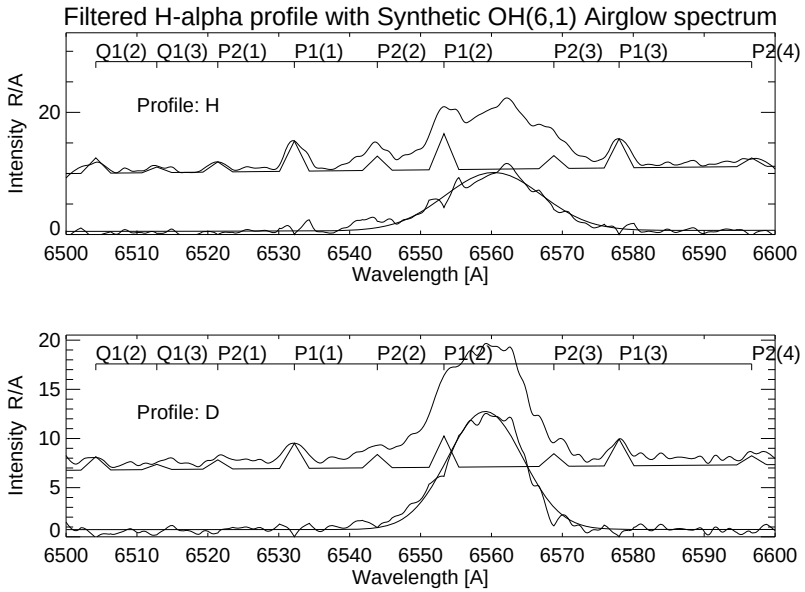

Figure 7.1: Fit of measured H_α profiles without the OH(6,1) contribution

H_α	a_0	a_1	a_2	a_3	a_4	a_5	Tot. int.
Index	$R/\mathring{A}$	$\mathring{A}$	$\mathring{A}$	$R/\mathring{A}$	$R/\mathring{A}^2$	$R/\mathring{A}^3$	R
$\mathcal{H}$	9.5	6560.3	6.8	-80.4	0.02	-1.6E-06	224.2
$\mathcal{D}$	11.9	6559.1	5.3	-59.6	0.02	-1-4E-06	233.9

Table 7.1: Parameters to fitted H_α profiles without the OH(6,1) contribution.

7.2 Comparison

Comparing modelled H_α and H_β Doppler broadened and shifted hydrogen line profiles with measured profiles, the modelled profiles are given in relative intensity values and without noise. To get the same peak intensity in the modelled compared to the measured profiles, a variable factor is used until the best fit is obtained. The

interesting thing to compare is the shape of the modelled profile compared to the measured. We have some degree of freedom determining the shape of the modelled profiles by adding up the contributions from each height level of the atmosphere, c.f. equation (4.5),

$$I_\chi(E_{SE}) = \sum_h J_\chi(h, E_{SE}) \cdot \Delta s.$$

Simulations described in chapter 4 told that the height integrated profiles became wider and more shifted towards the blue when the proton spectrum on the top of the atmosphere consisted of more "high energetic protons", compared to a more soft proton spectrum consisting of "low energetic protons".

Normalizing the modelled profiles, and multiply by a factor k,

$$I_{norm}(\lambda) = (\frac{(I(\lambda) - I_{min}(\lambda))}{(I_{max}(\lambda) - I_{min}(\lambda))}) \cdot k,$$

and plot in the same coordinate system as the measured profiles, we may compare theory and measurements.
Fig. 7.2 shows a plot of the measured profile $\mathcal{H}$, both H_α and H_β, viewed at 71° relative to the magnetic field, and the corresponding modelled profiles for isotropic and cosine-dependent pitch angle distributions. The modelled profiles are height integrated down to 105 km. The modelled H_α profile seems to fit the measured profile pretty good, especially the one with a cosine dependent pitch angle distribution. But the modelled H_β profiles are too wide compared to the measured, and there is obvious disagreement in the shortwavelength side of H_β. It seems that the background correction is not sufficient.

Since the H_α profile measured at the view angle of 71° relative to the magnetic field and the corresponding modelled profile fitted well, the same height interval for the profiles modelled at 19° relative to the magnetic field is assumed. The result is shown in Fig. 7.3.

The H_α model and measured profile fit is not satisfactorily. The cosine model profile should have been shifted a few $\mathring{A}$ towards higher wavelengths, and be more flat around the top. It might result from a more complex input spectrum or a mixture of several well–define spectra.

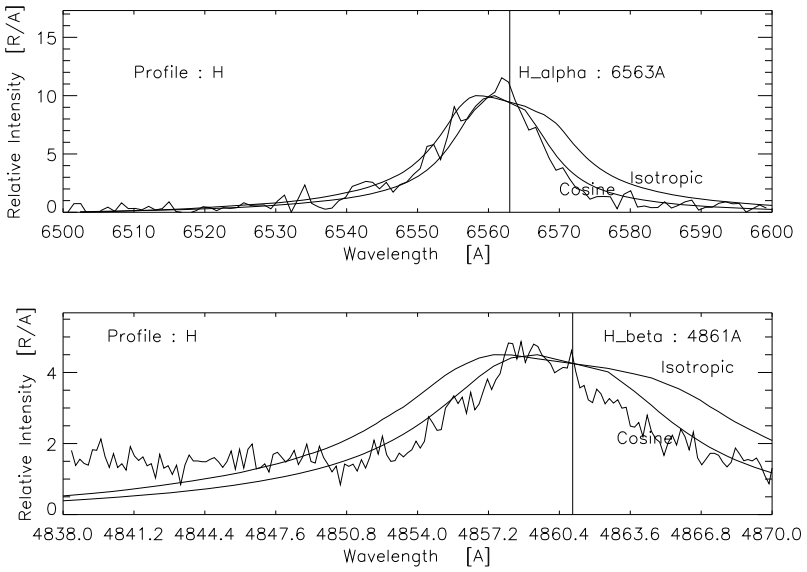

Figure 7.2: Measured and modelled H_α and H_β profiles viewed at 71° relative to the magnetic field

We must also have in mind that we assumed a normalized cosine pitch angle distribution, under the assumption that the main part of the protons were close to the magnetic field line. If we assume an isotropic pitch angle distribution, we should have a larger contribution from emitters not so close to the magnetic field line. That is, all solutions in Fig. 4.3 with the corresponding numbers of emitters will contribute more to the line of sight energy than in the case of a cosine-dependent pitch angle distribution. The number of emitters at an arbitrary height will be the same as on top of the atmosphere, if they are not already stopped. Thus the modelled profiles would get wider. This effect is shown in Fig. 7.3 and 7.2. The 'isotropic' profiles are wider than the 'cosine' profiles. Thus, it seems like the best fit of the measured H_α and H_β profiles $\mathcal{D}$ is obtained when the pitch angle distribution is assumed cosine. But the low intensities of the H_β profiles make it difficult to determine any significant shape, and hence it is difficult to compare with modelled profiles. As in Fig. 7.2 the fit in the low–wavelength shoulder of H_β is not satisfactory. It must be realized that the H_α and H_β spectra were obtained simultaneously for each view angle. Changing the input spectrum will have consequences for the fits of both measured profiles, and this is a main constraint. However, our fitting procedure may be improved, and future studies have to advance the algorithms and

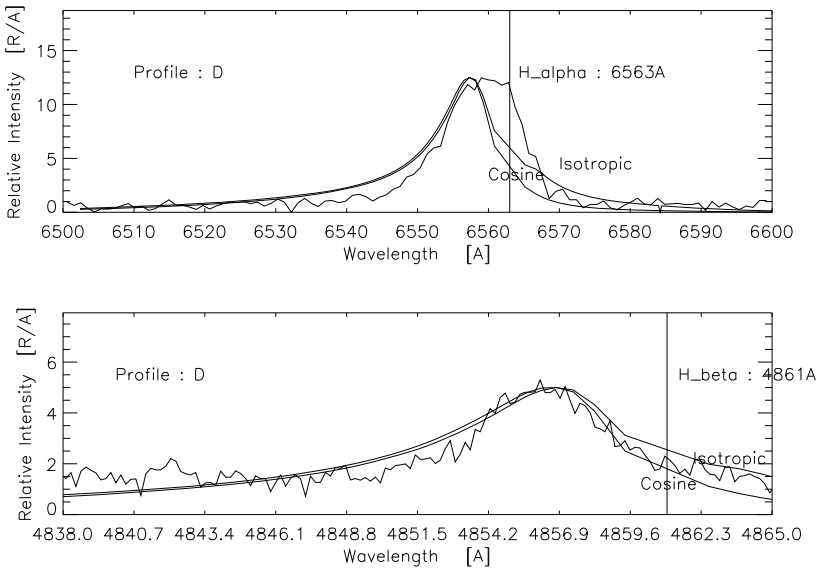

Figure 7.3: Measured and modelled H_α and H_β profiles viewed at 19° relative to the magnetic field

computer work.

So, we could adjust the modelled profiles to the measured profiles by trying different pitch angle distributions and proton spectra on top of the atmosphere. If a proton spectrum was measured, then it would be highly possible that both energy and pitch–angle distributions were obtained. Our program require too much computing time to search through several possible energy and pitch–angle spectra to get the input data which match the measured Doppler profile most satisfactorily. For future work the schedule must be to measure the Doppler profiles closely. Using our analytical procedure, it can be possible to get information of the incoming proton spectrum. The real test of this method is simultanous space measurements of the proton spectrum, in situ (rocket) measurements of the volume emission rate, and ground–based measurements of the integrated Doppler profile. Even if these calculations are carried out only with one proton spectrum as input, the atmospheric modulation of the input proton spectrum may be considered as general, and must be a key subject also in future research. In order to be decisive also measurements have to be carried out, and the physical complex interaction between protons and atmospheric species can not be solved by numerical calculations on high–speed computers alone.

Chapter 8

Conclusions

We have studied the Doppler shifted and broadened auroral hydrogen line profiles, H_α and H_β, by first using empirical energy–range relations for protons in air to obtain the energy loss, and then using these relations to calculate how a given proton spectrum changes as a function of height. All calculations are two–dimesional.
Calculations showed us that a proton spectrum with a low energy tail at the top of the atmosphere (*Reasoner et al.*, 1968), assuming a cosine pitch–angle distribution, did not change shape at heights above 150 km, because there is no significant energy loss of the penetrating protons. The proton spectrum at the top was assumed to be a narrow incoming beam. Below 150 km the proton spectrum changed, especially the low energy tail. This tail was connected to the Maxwellian–like distribution as an additional low–energy peak. This, because the low energy protons are stopped faster than those with higher energy. We also had a shift of the high energy Maxwellian–like distribution towards lower energies when the height decreased.
When we had calculated the effective emission rate for H_α, we could study the corresponding emission rate distribution as a function of height. Calculations showed us that the low energy tail in the proton distribution gave us a corresponding emission peak in the emission rate distribution. This, because the low energy (H^+/H)–particles emit most light. The emission rate distribution had an increasing maximum shifted towards higher energies, when the particles travelled into the atmosphere. But at a certain height, in our case 115 km, this maximum started to decrease

quickly.

After constructing the simple model of calculating the Doppler shifted and broadened hydrogen line profiles, H_α and H_β, viewed at arbitrary angles with the magnetic field, using a different proton energy spectra, we could see similar effects. At heights close to 150 km, where the loss of protons is low, the modelled profiles became narrow. It is reasonable to assume that these profiles were a result of the low energetic tail of the proton spectrum. The maximum of the profiles increased and got shifted towards lower wavelengths for decreasing height. But at a certain height, in our case at 110 km, this maximum decreased quickly. The profiles also became wider as we went deeper into the atmosphere. From this, it must be reasonable to assume that narrow Doppler profiles with little shift must be result from soft incoming proton spectra. Wide profiles must result from hard proton spectra.
We also found out that the width of the modelled profiles became wider with an isotropic pitch–angle distribution compared with a cosine pitch–angle distribution. This, because we will have a larger contribution to the profile from emitters not so close to the magnetic field line when we assume an isotropic pitch–angle distribution compared to a cosine pitch–angle distribution.

Ground–based spectroscopic observation of auroral H_β and H_α at different view angles with the magnetic field were made during January 1991 at Nordlysstasjonen, using two high resolution Ebert–Fastie spectrometers. A comparison between the measured profiles and the modelled profiles and the resulting fit showed us that it is possible to find reasonable input pitch–angle distributions and proton spectra. Since the measured profiles were narrow and low in intensity, which is usual at high latitudes, we have to use an adequately soft proton energy distribution at the top of the atmosphere as an input to our model in order to get an acceptable coincidence between the measurements and the model.

The model may be improved by applying a two–dimensional Proton–Hydrogen transport model instead of the calculations made in chapter 2. However, parameters of this model need to be confirmed by in situ measurements of the degradation of the proton flux in the atmosphere. In our case we have based our analysis on physical

knowledge about proton interaction with atmospheric species and measured spectra. Then we have avoided the hard numerical calculations which can be hard to verify by data.

By our procedure we have gained new insight in the physical processes leading to the observed hydrogen profiles. In future we hope to be able to continue this work, make our model 3–dimensional, use a converging geomagnetic field, and study eventual improved fits to data. We have much more technical equipment than the auroral pioneers as *Vegard*, and by this work we have shown how the technical equipment can be used. Auroral studies are complex, but exciting and we are aiming for decades in this field as *Lars Vegard*.

Appendix A

The turbo pascal unit XYPLOT

XYPLOT UNIT , VERSION 2
RELEASE 2
RELEASE NOTES

Graphics procedures:
Initxyplot
Closexyplot
Definewindow
Xtitle
Ytitle
Title
TexStringLabel
ClearTexStringLabel
ClearWindow
ClearScreen
Plot
DrawLine
PostScriptScreen

while Turbo Pascal version 5.0 provides some built-in graphics capabilities , they do not come close to providing a complete graphics library.

This unit is made with the help of the Graph.tpu file which is a unit that Turbo Pascal provides. The procedures in this unit is ment to make it easier to do some simple plotting when you are programming in Turbo Pacsal. The following is a quick reference to the procedures contained in the XYplot unit.

XYPLOT UNIT PROCEDURES

INITXYPLOT
Syntax
Procedure initxyplot(BackgroundColor:integer);
Usage
Clears screen and sets the computer to graphics mode. It does not initialize the graphics system.

CLOSEXYPLOT
Syntax
Procedure closexyplot;
Usage
It leaves the graphic mode and returns to Text mode.

DEFINEWINDOW
Syntax
Procedure definewindow(windowcolor:word;x1,y1,x2,y2:integer;xmin,xmax,ymin,ymax:real)
x1,y1,x2,y2:Upper and Lower corner in screen-coordinates.
xmin,xmax,ymin,ymax:World-coordinates.
Usage
It defines the area on the screen and initializes the coordinate-system for the user.

XTITLE
Syntax
Procedure xtitle(TextColor:word;Text:string);
Usage
Enter Textlabel on x-axsis in specified color.

YTITLE
Syntax
Procedure ytitle(TextColor:word;Text:string);
Usage
Enter Textlabel on y-axsis in specified color.

TITLE
Syntax
Procedure title(Textcolor:word;Text:string);
Usage
Enter Textlabel on top of plot in specified color.

TEXSTRINGLABEL
Syntax
Procedure textstringlabel(Textsize,Textcolor,X,Y:integer,Text:string);
Usage
Enter Text in world-coordinates.

CLEARTEXSTRINGLABEL
Syntax
Procedure cleartextstringlabel(backgroundcolor,X,Y,Textsize:integer);
Usage
This procedure clears or overwrites anything on the screen when world-coordinates are specified with given Textlenght.

CLEARWINDOW

Syntax
Procedure clearwindow;
Usage
Clears entire window.

CLEARSCREEN
Syntax
Procedure clearscreen;
Usage
Clears entire screen.

PLOT
Syntax
Procedure plot(AxisColor,PlotColor:word;var X,Y:vector;lengthofvector:integer);
Usage
vector:array[1..2000] of reals;
X and Y same length.
plots in colors the arrays X and Y with the given length.

DRAWLINE
Syntax
Procedure drawline(LineColor:word,x1,y1,x2,y2:real);
Usage
Draws a line from the world-coordinates (x1,y1) to (x2,y2) with specified color.

POSTSCRIPTSCREEN
Syntax
Procedure postscriptscreen(postscriptscreenfilename:string);
Usage
Dumps the PC-screen in graphics mode to a postscript file. (Monochrome). Compatible with LaTex.

Printers

You may want to get a Hard-copy of your screen. This can be done by using the postscriptscreen procedure explained above. Else you can use a line printer by including dump.pas to your pascal program. If you have a Hp-Laser printer then you just use the Shift-Print Scrn option with the prtscrff.com and graphics.com in Dos.

Appendix B

Listing of the program PROFILE.P

This program calculates the H_α or the H_β profile viewed at an arbirary angle with the magnetic field at height h.
The program is written in pascal.

```
program profile(input,output,Elossdata,profiledata,howfar);
Const NrSightE=200;
      pi=3.141592654;
type
     Zerotype=array[1..2] of real;
     SightEtype=array[1..NrSightE] of real;

var  Elossdata,profiledata,howfar:Text;
     Eloss,h,ro,O2,N2,theta0,deltaEH:real;
     IndexSightE,NrZeroes,testlight:integer;
     SE,EH,ViewAngel,Counts,Emissions,EHloop:real;
     Zeroes:Zerotype;
     SightE:SightEtype;
     light,Legaltheta0:boolean;

procedure ElossRead(hight:integer;var h,Eloss,O2,N2,ro:real);
var t1,t2,t3,t4,t5:real;
      finished:boolean;
begin
   reset(Elossdata,'eloss.dat');
   finished:=false;
   while not finished do
   begin
     readln(Elossdata,t1,t2,t3,t4,t5);
     if round(t1)= hight then
     begin
       h:=t1;Eloss:=t2;O2:=t3;N2:=t4;ro:=t5;
       finished:=true;
     end;
   end;
   close(Elossdata);
end;

function Rad(theta:real):real;
begin
   Rad:=pi*theta/180.0;
end;

function Op(E:real;n:real):real;
begin
   Op:=exp(n*ln(E));
end;
```

```
function n(theta:real):real;
begin
    n:=1/pi;
   -n:=0.5*cos(Rad(theta));"
end;

function FH(EH:real):real;
var temp:real;
begin
   if EH¡100 then temp:=2*pi*8.0E+07*exp(-2*ln(EH));
   if EH¿=100 then temp:=2*pi*2.0E+17*exp(-6.67*ln(EH));
   FH:=temp;
end;

procedure EmissionRate(E:real;Zero:real;EH:real;var EmissionZeropoint:real);
var m,sigmaeff:real;
function On2hb(E:real):real;
var temp:  real;
    A1,A2,A3,A4,A5,A6,B1,B2,B3,B4,C1,C2,C3,C4,C5,C6,
    D1,D2,D3,D4,D5,D6,E1,E2,E3,E4,E5,E6:  real;
begin
   -FitCoeff of N2hb Cross-Section"
   -Energy int.:0.03-1.60"
   A1:=-3.12465311985870E+0001;
   A2:= 1.84656146273203E+0003;A3:=-1.95372556990013E+0002;
   A4:=-2.53357589619607E+0003;A5:= 2.22618224956468E+0003;
   A6:=-5.65465492459014E+0002;
   -Energy int.:1.60-4.00"
   B1:= 9.69167928806506E+0002;
   B2:=-2.30978390818229E+0002;B3:= 4.68802886185586E+0001;
   B4:=-3.46474240050884E+0000;
   -Energy int.:3.20-12.50"
   C1:= 7.36714115995914E+0002;
   C2:=-5.11167642662185E+0001;C3:= 8.51653624733444E-0001;
   C4:= 6.51117846297893E-0001;C5:=-6.83019986969384E-0002;
   C6:= 2.06154175663187E-0003;
   -Energy int.:12.50-160.00"
   D1:= 4.51929314279929E+0002;
   D2:= 3.95005985745593E+0000;D3:=-3.01874924371077E-0001;
   D4:= 4.26461137135448E-0003;D5:=-2.51872401435815E-0005;
   D6:= 5.45916883554123E-0008;
   -Energy int.:160.00-800.00"
   E1:= 3.24945595474448E+0002;
   E2:=-3.46940719141276E+0000;E3:= 1.47755278523363E-0002;
   E4:=-3.08415512645932E-0005;E5:= 3.13048820206716E-0008;
   E6:=-1.23205646035850E-0011;
   if (E¡0.032) then temp:=0;
   if (E¿=0.032) and (E¡=1.6) then
   temp:=A1+A2*E+A3*Op(E,2)+A4*Op(E,3)+A5*Op(E,4)+A6*Op(E,5);
   if (E¿1.6) and (E¡=4.0) then
   temp:=B1+B2*E+B3*Op(E,2)+B4*Op(E,3);
   if (E¿4.0) and (E¡=12.5) then
   temp:=C1+C2*E+C3*Op(E,2)+C4*Op(E,3)+C5*Op(E,4)+C6*Op(E,5);
   if (E¿12.5) and (E¡=160) then
   temp:=D1+D2*E+D3*Op(E,2)+D4*Op(E,3)+D5*Op(E,4)+D6*Op(E,5);
   if (E¿160) and (E¡=800) then
   temp:=E1+E2*E+E3*Op(E,2)+E4*Op(E,3)+E5*Op(E,4)+E6*Op(E,5);
   if (E¿800) then temp:=0;
  On2hb:=temp;
end;
function Oo2hb(E:real):real;
var temp:real;
    A1,A2,A3,A4,B1,B2,B3,B4,C1,C2,C3,C4,
    D1,D2,D3,D4,E1,E2,E3,E4,E5,E6:  real;
begin
    -FitCoeff of O2hb Cross-Section"
    -Energy int.:0.03-1.25"
    A1:=-4.42372224541614E+0001;
    A2:= 1.36033581919782E+0003;A3:=-1.26533483294584E+0003;
    A4:= 4.05074811487459E+0002;
    -Energy int.:1.25-3.20"
    B1:= 4.27449644570239E+0002;
    B2:= 4.42412554791081E+0001;B3:=-6.03731458447874E+0000;
    B4:=-1.17693084510574E+0000;
    -Energy int.:3.20-12.50"
    C1:= 5.75022693724371E+0002;
    C2:=-4.15981316558318E+0001;C3:= 2.97826743267069E+0000;
    C4:=-7.88770994463448E-0002;
    -Energy int.:12.50-160.00"
    D1:= 4.23430453221314E+0002;
    D2:=-4.61726432150317E+0000;D3:= 1.22573686843594E-0002;
    D4:= 8.69584849853833E-0006;
    -Energy int.:160.00-800.00"
    E1:= 2.54492103698431E+0002;
    E2:=-2.71333710705221E+0000;E3:= 1.15420524011540E-0002;
    E4:=-2.40695734582130E-0005;E5:= 2.44131744310820E-0008;
    E6:=-9.60274624184685E-0012;
    if (E¡0.032) then temp:=0;
```

```
    if (E¿=0.032) and (E¡=1.25) then
    temp:=A1+A2*E+A3*Op(E,2)+A4*Op(E,3);
    if (E¿1.25) and (E¡=3.2) then
    temp:=B1+B2*E+B3*Op(E,2)+B4*Op(E,3);
    if (E¿3.2) and (E¡=12.5) then
    temp:=C1+C2*E+C3*Op(E,2)+C4*Op(E,3);
    if (E¿12.5) and (E¡=160) then
    temp:=D1+D2*E+D3*Op(E,2)+D4*Op(E,3);
    if (E¿160) and (E¡=800) then
    temp:=E1+E2*E+E3*Op(E,2)+E4*Op(E,3)+E5*Op(E,4)+E6*Op(E,5);
    if (E¿800) then temp:=0;
    Oo2hb:=temp;
end;
function On2ha(E:real):real;
var temp:real;
    A1,A2,A3,A4,A5,A6,B1,B2,B3,B4,C1,C2,C3,C4,C5,C6,
    D1,D2,D3,D4,D5,D6,E1,E2,E3,E4,E5,E6:  real;
begin
  -FitCoeff of N2ha Cross-Section"
  -Energy int.:0.03-1.25"
  A1:= 1.30756432234077E+0002;
  A2:= 5.21538443852961E+0003;A3:= 2.16879481588900E+0004;
  A4:=-5.74625014908314E+0004;A5:= 4.73095456253886E+0004;
  A6:=-1.32237962869406E+0004;
  -Energy int.:1.25-3.20"
  B1:= 4.78516472154856E+0003;
  B2:=-1.22431260586157E+0003;B3:= 1.13407759172493E+0002;
  B4:= 1.08466185525613E+0001;
  -Energy int.:3.20-12.50"
  C1:= 4.04701860236749E+0003;
  C2:=-9.13428832691163E+0002;C3:= 1.69431293056114E+0002;
  C4:=-1.71925145752321E+0001;C5:= 9.06819319519855E-0001;
  C6:=-1.95426724854144E-0002;
  -Energy int.:12.50-160.00"
  D1:= 1.56415853538550E+0003;
  D2:= 2.43914839063946E+0001;D3:=-1.38354868709757E+0000;
  D4:= 1.90830834891074E-0002;D5:=-1.12254203207374E-0004;
  D6:= 2.43305239797011E-0007;
  -Energy int.:160.00-800.00"
  E1:= 1.23100933697633E+0003;
  E2:=-1.31099667436793E+0001;E3:= 5.56856041849301E-0002;
  E4:=-1.15958519338211E-0004;E5:= 1.17464071656319E-0007;
  E6:=-4.61540473561053E-0011;
  if (E¡0.032) then temp:=0;
  if (E¿=0.032) and (E¡=1.25) then
  temp:=A1+A2*E+A3*Op(E,2)+A4*Op(E,3)+A5*Op(E,4)+A6*Op(E,5);
  if (E¿1.25) and (E¡=3.2) then
  temp:=B1+B2*E+B3*Op(E,2)+B4*Op(E,3);
  if (E¿3.2) and (E¡=12.5) then
  temp:=C1+C2*E+C3*Op(E,2)+C4*Op(E,3)+C5*Op(E,4)+C6*Op(E,5);
  if (E¿12.5) and (E¡=160) then
  temp:=D1+D2*E+D3*Op(E,2)+D4*Op(E,3)+D5*Op(E,4)+D6*Op(E,5);
  if (E¿160) and (E¡=800) then
  temp:=E1+E2*E+E3*Op(E,2)+E4*Op(E,3)+E5*Op(E,4)+E6*Op(E,5)+E6;
  if (E¿800) then temp:=0;
  On2ha:=temp;
end;
function Oo2ha(E:real):real;
var temp:real;
    A1,A2,A3,A4,A5,A6,B1,B2,B3,B4,C1,C2,C3,C4,C5,C6,
    D1,D2,D3,D4,D5,D6,E1,E2,E3,E4,E5,E6:  real;
begin
  -FitCoeff of O2ha Cross-Section"
  -Energy int.:0.03-1.25"
  A1:=-1.57163911024341E+0002;
  A2:= 7.24472228805721E+0003;A3:=-8.70291068643332E+0002;
  A4:=-1.56906267278939E+0004;A5:= 1.73735587673485E+0004;
  A6:=-5.57366351245344E+0003;
  -Energy int.:1.25-3.20"
  B1:= 2.61096992056072E+0003;
  B2:=-2.73357057642657E+0002;B3:= 1.96993173282826E+0001;
  B4:=-8.57787790131624E-0001;
  -Energy int.:3.20-12.50"
  C1:= 2.83331775543466E+0003;
  C2:=-4.52524431727827E+0002;C3:= 6.98202678306261E+0001;
  C4:=-7.19720044030691E+0000;C5:= 4.62183249160717E-0001;
  C6:=-1.29335954557632E-0002;
  -Energy int.:12.50-160.00"
  D1:= 1.46341331630573E+0003;
  D2:=-5.68926549036405E+0000;D3:=-2.86337164387987E-0001;
  D4:= 3.99889755860272E-0003;D5:=-2.06134382963186E-0005;
  D6:= 3.84422898944354E-0008;
  -Energy int.:160.00-800.00"
  E1:= 9.70147945162840E+0002;
  E2:=-1.03279336760897E+0001;E3:= 4.38573782482763E-0002;
  E4:=-9.13147074056431E-0005;E5:= 9.24959756654162E-0008;
  E6:=-3.63442106664295E-0011;
  if (E¡0.032) then temp:=0;
```

```
   if (E¿=0.032) and (E¡=1.25) then
   temp:=A1+A2*E+A3*Op(E,2)+A4*Op(E,3)+A5*Op(E,4)+A6*Op(E,5);
   if (E¿1.25) and (E¡=3.2) then
   temp:=B1+B2*E+B3*Op(E,2)+B4*Op(E,3);
   if (E¿3.2) and (E¡=12.5) then
   temp:=C1+C2*E+C3*Op(E,2)+C4*Op(E,3)+C5*Op(E,4)+C6*Op(E,5);
   if (E¿12.5) and (E¡=160) then
   temp:=D1+D2*E+D3*Op(E,2)+D4*Op(E,3)+D5*Op(E,4)+D6*Op(E,5);
   if (E¿160) and (E¡=800) then
   temp:=E1+E2*E+E3*Op(E,2)+E4*Op(E,3)+E5*Op(E,4)+E6*Op(E,5);
   if (E¿800) then temp:=0;
   Oo2ha:=temp;
end;
procedure FinnSigmaEff(E:real;Line:integer;var sigmaeff:real);
var FraktN2,FraktO2:real;
begin
    FraktO2:=(O2/(O2+N2));
    FraktN2:=(N2/(O2+N2));
    case Line of
      4861:sigmaeff:=0.279*(FraktN2*On2hb(E)+FraktO2*Oo2hb(E))*1E-20;
      6563:sigmaeff:=0.442*(FraktN2*On2ha(E)+FraktO2*Oo2ha(E))*1E-20;
    end;
end;
begin
    m:=((1.6021E-16/1.67E-27)*100*100*2);
    FinnSigmaEff(E,6563,sigmaeff);
    emissionZeropoint:=((O2+N2)*sigmaeff*sqrt(E*m))*FH(EH)*n(Zero);
end;

function E(theta:real;EH:real;Eloss:real):real;
begin
    E:=(EH-(1/cos(Rad(theta)))*Eloss);
end;

function f(theta:real;EH:real;SE:real;ViewAngel:real;Eloss:real):real;
begin
 f:=(EH-(1/cos(Rad(theta)))*Eloss)*cos(Rad(ViewAngel-theta))-SE;
end;

procedure FindZeroes(SE:real;EH:real;tetha0:real;ViewAngel:real;
                     var Zeroes:Zerotype;var NrZeroes:integer);
var a,b,Zeropoint,delta:real;
                  j:integer;
              Leagal:boolean;
procedure Secant(p0,p1:real;var Zeropoint:real);
var Tol,q0,q1,p:real;
    find:boolean;
    k,N0:integer;
begin
    N0:=1000;
    Tol:=1E-03;find:=false;k:=1;
    q0:=f(p0,EH,SE,ViewAngel,Eloss);
    q1:=f(p1,EH,SE,ViewAngel,Eloss);
    while (not find) and (k¡=N0) do
    begin
       p:=p1-q1*(p1-p0)/(q1-q0);
       if abs(p-p1)¡Tol then
       begin
           Zeropoint:=p;
           find:=true;
       end;
     p0:=p1;q0:=q1;p1:=p;q1:=f(p,EH,SE,ViewAngel,Eloss);k:=k+1;
   end;
end;
begin
   delta:=1;
   j:=0;Leagal:=true;
   a:=-tetha0;b:=a+delta;
   while  Leagal do
   begin
      if ((f(a,EH,SE,ViewAngel, Eloss)*f(b,EH,SE,ViewAngel, Eloss))¡0) then
      begin
          Secant(b-delta,b,Zeropoint);
          if (E(Zeropoint,EH,Eloss)¿=0) and (abs(Zeropoint)¡=90) then
          begin
             j:=j+1;
             Zeroes[j]:=Zeropoint;
             if j=2 then Leagal:=false;
             a:=b;
          end;
      end;
    b:=b+delta;
   if (b¿tetha0) then Leagal:=false;
  end;
 NrZeroes:=j;
end;

procedure FindEmissions(NrZeroes:integer;Zeroes:Zerotype;EH:real;
```

```
                                Eloss:real;var Emissions:real);
var EE,EmissionZeropoint:real;
    i:integer;
begin
      if NrZeroes¿0 then
      begin
        Emissions:=0;
        for i:=1 to NrZeroes do
        begin
          EE:=E(Zeroes[i],EH,Eloss);
          EmissionRate(EE,Zeroes[i],EH,EmissionZeropoint);
          Emissions:=Emissions+EmissionZeropoint;
        end;
      end
      else
        begin
          Emissions:=0;
        end;
end;

procedure FindTheta0(EH:real;Eloss:real;var theta0:real;
                              var Legaltheta0:boolean);
var tetta:real;
    finished:boolean;
begin
     tetta:=90; finished:=false;
     while (not finished) and (tetta¿=0) do
     begin
       tetta:=tetta-0.1;
       if (EH-(1/cos(Rad(tetta)))*Eloss)¿0 then
       begin
           theta0:=tetta;
           finished:=true;
       end;
     end;
     if theta0¡0 then Legaltheta0:=false
     else Legaltheta0:=true;
end;

procedure MakeSightE(var SightE:SightEtype);
var i,hs1,hs2:integer;
    temp1,temp2,temp3:array[1..NrSightE] of real;
begin
    hs1:=NrSightE div 2;
    hs2:=hs1 div 2;
    for i:=1 to hs1 do temp1[i]:=(10/(hs1-1))*i-5-(10/(hs1-1));
    for i:=1 to hs2 do temp2[i]:=(35/(hs2-1))*i+5-(35/(hs2-1));
    for i:=1 to hs2 do temp3[i]:=(35/(hs2-1))*i-40-(35/(hs2-1));
    for i:=1 to NrSightE do
    begin
      if (i¡=hs2) then SightE[i]:=temp3[i];
      if (i¿hs2) and (i¡=(hs1+hs2)) then SightE[i]:=temp1[i-hs2];
      if (i¿(hs1+hs2)) then SightE[i]:=temp2[i-(hs1+hs2)];
    end;
end;

procedure ReWriteProfiledata;
begin
    rewrite(profiledata,'155ha19ISO.dat');
end;

procedure WriteToProfiledata(var SE,Counts:real;deltaEH:real);
begin
    writeln(profiledata,SE,' ',Counts);
    rewrite(howfar,'hfISO.dat');
    writeln(howfar,SE,' ',Counts*deltaEH);
    close(howfar);
end;

-BEGIN MAIN"
begin
  ViewAngel:=19;
  ElossRead(155,h,Eloss,O2,N2,ro);
  ReWriteProfiledata;
  MakeSightE(SightE);
  IndexSightE:=1;
  deltaEH:=0.01;
  while (IndexSightE¡=NrSightE) do
  begin
    SE:=SightE[IndexSightE];
    EH:=abs(SE);light:=true;Counts:=0;testlight:=1;EHloop:=0;
    while light do
    begin
      FindTheta0(EH,Eloss,theta0,Legaltheta0);
      if Legaltheta0 then
      begin
       if (testlight mod 10 =0) and (counts¡¿0) then EHloop:=Counts;
       if (testlight mod 10 ¡¿0) and (Counts¡¿0)
```

```
        and (abs(Counts-EHloop)¡=10000) then light:=false;
        if (ViewAngel=0) and (SE¡=0) then light:=false;
        if (NrZeroes=0) and (EH¿500) then light:=false;
        FindZeroes(SE,EH,theta0,ViewAngel,Zeroes,NrZeroes);
        FindEmissions(NrZeroes,Zeroes,EH,Eloss,Emissions);
        Counts:=Counts+Emissions;
        testlight:= testlight+1;
       end;
       EH:=EH+deltaEH;
    end;
    WriteToProfiledata(SE,Counts,deltaEH);
    IndexSightE:=IndexSightE+1;
  end;
  close(profiledata);
end.
-END MAIN"
```

Appendix C

Listing of the program SYNTHETICOH.PRO

This program makes a synthetic OH(6,1) spectrum. And it is used for filtering out the OH(6,1) contribution in the measured H_α profiles.
The program is written in IDL : Interactive Data Language.

```
function G,v
G=3737.9*(v+0.5) - 84.965*(v+0.5)^2 + 0.5398*(v+0.5)^3 -
  0.01674*(v+0.5)^4 - 0.001637*(v+0.5)^5
return,G
end

function B,v
B=18.867-0.708*(v+0.5)+0.00207*(v+0.5)^2
return,B
end

function D,v
D=0.0018
return,D
end

function F1,J
Y6=-9.795
F1=(B(6.0) * ((J + 0.5)^2. - 1 - 0.5 * sqrt(4. * (J + 0.5)^2. +
   Y6 * (Y6 - 4.))) - D(6.0) * J^4.)
return,F1
end

function F11,J
Y1=-7.876
F1=(B(1.0) * ((J + 0.5)^2. - 1 - 0.5 * sqrt(4. * (J + 0.5)^2. +
   Y1 * (Y1 - 4.))) - D(1.0) * J^4.)
return,F1
end

function F2,J
Y6=-9.795
F2=(B(6.0) * ((J + 0.5)^2 - 1 + 0.5 * sqrt(4. * (J + 0.5)^2. +
   Y6 * (Y6 - 4.))) - D(6.0) * (J+1.)^4.)
return,F2
end

function F21,J
Y1=-7.876
F2=(B(1) * ((J + 0.5)^2 - 1 + 0.5 * sqrt(4. * (J + 0.5)^2. +
   Y1 * (Y1 - 4.))) - D(1.0) * (J+1.)^4.)
return,F2
```

```
end

Pro Readdatafile,filename,Aangstrom,Counts
openr,1,filename
A=fltarr(2,104)
readf,1,A
Aangstrom=A(0,*)
Counts=A(1,*)
close,1
return
end

Pro Info'OH'filter
print,'Filters the OH(6.1)-contribution of the measured H'alpha profile'
print,'Plots & temperature & concentration & total intensities'
print,'Input: OH'filter,viewangle,Bandpass,Corr. Background,
          Temp?:(1)(2)(3),filename'
print,'The intensity is prop. with the factor N/Q'int'
return
end

Pro Fit,xxx,yyy,yfit
yfit=gaussfit(xxx,yyy,coef)
print,'Exponential Gaussfit :output Coef.:'
print,coef
return
end

function wave,K,J,J0
ny=fltarr(9)
for v=0,8 do begin
if (J(v)-K(v) EQ -0.5) then ny(v)=F'26(J(v))-F'21(J0(v))+G'v(6.0)-G'v(1.0)
else ny(v)=F'16(J(v))-F'11(J0(v))+G'v(6.0)-G'v(1.0)
endfor
my=((3.0E+08/((ny)*2.99792458E+10))*1E+10)
return,my
end

function wavenr,K,J,J0
my=fltarr(9)
for v=0,8 do begin
if (J(v)-K(v) EQ -0.5) then my(v)=F'26(J(v))-F'21(J0(v))+G'v(6.0)-G'v(1.0)
else my(v)=F'16(J(v))-F'11(J0(v))+G'v(6.0)-G'v(1.0)
endfor
return,my
end

Pro ReadVar,K,J,J0,A,eV,Boltz,lambda
;begin read from datafiles
openr,2,'syntheticOH.dat'
B=fltarr(5,9)
readf,2,B
close,2
lambda=B(0,*)
K=B(1,*)
J=B(2,*)
J0=B(3,*)
A=B(4,*)
;end read from datafiles
;begin constants in use
Boltz=8.61739D-05
eV=1.239842D-04
;end constants in use
return
end

Pro Text,wavelenght,Intensity
pos=(2*max(Intensity)-max(Intensity)/4)
B=wavelenght
XYouts,B(0),pos,'Q1(2)'
XYouts,B(1),pos,'Q1(3)'
XYouts,B(2),pos,'P2(1)'
XYouts,B(3),pos,'P1(1)'
XYouts,B(4),pos,'P2(2)'
XYouts,B(5),pos,'P1(2)'
XYouts,B(6),pos,'P2(3)'
XYouts,B(7),pos,'P1(3)'
XYouts,B(8),pos,'P2(4)'
pos=2*max(Intensity)-max(Intensity)/3.5
delta=max(Intensity)/16
Plots, [B(0),B(8)], [Pos,Pos]
for v=0,8 do Plots, [B(v),B(v)], [Pos,Pos-delta]
return
end

function O'2,Temp,ev,Boltz
sum=0
for v=1,40 do begin
```

```
w=v-0.5
sum=sum+(2*w+1)*exp((-1.0*F`26(w)*eV)/(Boltz*Temp))
endfor
return,sum
end

function O`1,Temp,ev,Boltz
sum=0
for v=1,40 do begin
w=v+0.5
sum=sum+(2*w+1)*exp((-1.0*F`16(w)*eV)/(Boltz*Temp))
endfor
return,sum
end

function partG,Temp,ev,Boltz
sum=0
for v=0,10 do begin
sum=sum+exp(-1*(G`v(v)*ev)/(Temp*Boltz))
endfor
return,sum
end

Pro MakeX,x
x=findgen(3001)*0.1+6400.0
x=x(where( x GE 6500. and x LE 6600.))
return
end

Pro FindTemp1,Ip1,Ips1,J,A,ev,Boltz,Temp1
Temp1=((F`26(J(2))-F`16(J(3)))*ev/Boltz)/(Alog((Ips1*A(2)*
     (2*J(2)+1))/(Ip1*A(3)*(2*J(3)+1))))
return
end

Pro FindTemp2,Ip1,Ip4,J,A,ev,Boltz,Temp2
Temp2=((F`26(J(2))-F`26(J(8)))*ev/Boltz)/(Alog((Ip4*A(2)*
     (2*J(2)+1))/(Ip1*A(8)*(2*J(8)+1))))
return
end

Pro FindTemp3,Ips1,Ips3,J,A,ev,Boltz,Temp3
Temp3=((F`16(J(3))-F`16(J(7)))*ev/Boltz)/(Alog((Ips3*A(3)*
     (2*J(3)+1))/(Ips1*A(7)*(2*J(7)+1))))
return
end

Pro Synthetic`OH,BP,Ips1,Ip1,Ip4,Ips3,T,viewangle,lambda,x,I
x=findgen(3001)*0.1+6400.0
info`oh`filter
;begin Syntethic OH
ReadVar,K,J,J0,A,eV,Boltz,lambda
FindTemp1,Ip1,Ips1,J,A,eV,Boltz,Temp1
FindTemp2,Ip1,Ip4,J,A,ev,Boltz,Temp2
FindTemp3,Ips1,Ips3,J,A,ev,Boltz,Temp3
NQtemp3=(Ips3/(A(7)* (2*J(7)+1)))*exp((F`16(J(7))*eV)/(Boltz*Temp3))
NQtemp1=(Ips1/(A(3)* (2*J(3)+1)))*exp((F`16(J(3))*eV)/(Boltz*Temp1))
NQtemp2=(Ip1/(A(2)* (2*J(2)+1)))*exp((F`26(J(2))*eV)/(Boltz*Temp2))
print,'NQP2(1)P1(1):',NQtemp1,'TempP2(1)P1(1):',Temp1
print,'NQP2(1)P2(4):',NQtemp2,'TempP2(1)P2(4):',Temp2
print,'NQP1(1)P1(3):',NQtemp3,'TempP1(1)P1(3):',Temp3
if T EQ 2 then begin
  N=NQtemp2
  Temp=Temp2
endif
 if T EQ 1 then begin
            N=NQtemp1
            Temp=Temp1
          endif else begin
                       N=NQtemp3
                       Temp=Temp3
                     endelse
part2rot=O`2(Temp,ev,Boltz)
part1rot=O`1(Temp,ev,Boltz)
partvib=partG(Temp,ev,Boltz)
!p.font=6
;begin calculate intensity
Intensity=fltarr(9)
for v=0,8 do begin
if (J(v)-K(v) EQ -0.5) then
Intensity(v)=N*A(v)* (2*J(v)+1) *exp( (-1.0*F`26(J(v))*eV)/(Boltz*Temp))
if (J(v)-K(v) EQ 0.5) then
Intensity(v)=N*A(v)*(2*J(v)+1)*exp( (-1.0*F`16(J(v))*eV)/(Boltz*Temp))
endfor
print,'Intensity of OH(6.1) (R) :'
for v=0,8 do print,(intensity(v)*BP)
;end calculate intensity
;begin calculate wavelenght
```

```
;Wavelenght=wave(K,J,J0)
;end calculate wavelenght
;begin convolution triangle
x=findgen(3001)*0.1+6400.0
I0=fltarr(3001)
for v=0,3000 do begin
 for w=0,8 do begin
   if ((v GT 0) AND (v LT 3000)) then begin
     if ((x(v-1) LT lambda(w)) AND (x(v+1) GT lambda(w))) then I0(v)=Intensity(w)
  endif
 endfor
endfor
xt=findgen(2*BP*10+1)*0.1
h=fltarr(2*BP*10+1)
for v=0,2*BP*10 do begin
if xt(v) LE xt(BP*10) then h(v)=(1/xt(BP*10))*xt(v)
else h(v)=(xt(v)-xt(2*BP*10))/(xt(BP*10)-xt(2*BP*10))
endfor
center=0
I=convol(I0,h,1)
I=I(where( x GE 6500. and x LE 6600.))
x=x(where( x GE 6500. and x LE 6600.))
;end convolution triangle
;end Synthetic OH
return
end

Pro Background,x,y,back,corrback
nrE=N_elements(x)
a=(( y(nrE-1)-y(0) )/( x(nrE-1)-x(0) ))
b=y(0)-a*x(0)
back=fltarr(nrE)
for v=0,nrE-1 do back(v)=a*x(v)+b+corrback
return
end

Pro integral,xx,yy,Answ
n=N_elements(xx)
D=xx(1)-xx(0)
sum=0
for v=0,n-1 do sum=sum+yy(v)
Answ=sum*D
return
end

Pro OH_filter,viewangle,BP,corrback,T,filename
Readdatafile,filename,Aangstrom,Counts
MakeX,x
y=Spline(Aangstrom,Counts,x)
Background,x,y,back,corrback
Ips1=y(where(x EQ 6532.20))-back(where(x EQ 6532.20))
Ips3=y(where(x EQ 6578.00))-back(where(x EQ 6578.00))
Ip1=y(where(x EQ 6521.40))-back(where(x EQ 6521.40))
Ip4=y(where(x EQ 6596.70))-back(where(x EQ 6596.70))
Synthetic_OH,BP,Ips1,Ip1,Ip4,Ips3,T,viewangle,lambda,x,I
I=I+back
plot,x,y,yrange=[0,2*(max(I))],/ystyle,Title='Filtered H-alpha profile with
Synthetic OH(6,1) Airglow spectrum',ytitle='Relative Intensity',
xtitle='Wavelength in Aangstroem'
Text,lambda,I
oplot,x,I
oplot,x,y-I
integral,x,y-I,Answ
print,'Total H-alpha intensity (R):',Answ
;Fit,x,y-I,yfit
;oplot,x,yfit
return
end
```

References

Barraclough, D. R. : 1987, 'International Geomagnetic Reference Field Revision 1987', *J. Geomag. Geoelectr.*, **39**, 773-779.

Bernstein, W., Inouye, G. T., Sanders, N. L. and Wax, R. L. : 1969, 'Measurements of precipitated 1- to 20-keV protons and electrons during a breakup aurora', *J. Geophys. Res.*, **74**, 3601.

Chamberlain, J. W. : 1961, 'Physics if the Aurora and Airglow', *Academic Press: New York.*

Cook, C. J., Jones, E., Jr. and Jorgensen, T., Jr. : 1953, 'Range-Energy Relations of 10- to 250-keV Protons and Helium Ions in Various Gases', *Phys. Rev.*, **91**, 1417.

Eather, R. H. and Jacka, F. : 1965, 'Auroral hydrogen emissions', *Aust. J. Phys.*, **19**, 241-274.

Ebert, H. : 1889, *Wied. Ann.*, **38**, 489.

Fastie, W. G. : 1952, 'A Small Plane Grating Monochromator', *J. Opt. Soc. Am*, **49**, 641.

Galperin, Yu. I. : 1963, 'Proton bombardment in aurora', *Planet. Space Sci.*, **10**, 187.

Giraud, A. and Petit, M. : 1978, 'Ionospheric Techniques and Phenomena', *D. Reidel Publ. co.: Holland.*

Hedin, A. E. : 1987, 'Neutral Thermosphere Model', *J. Geophys. Res.*, **92**, 4649.

Henriksen, K. : 1978, 'Variations of proton energy and pitch angle spectra in the upper atmosphere', *J. atmos. terr. Phys.*, **41**, 633-641

Henriksen, K., Fedorova, N. I., Totunova, G. F., Deehr, C. S., Romick, G. J. and Sivjee, G. G. : 1985, 'Hydrogen emissions in the polar cleft', *J. atmos. terr. Phys.*, **47**, 1051-1056.

Herzberg, G. : 1967, 'Spectra of Diatomic Molecules', *D. Van Nostrad co., inc.*

Hill, E. L. and Van Vleck, J. H. : 1923, *Physic. Rev.*, **32**, 250.

Krassovsky, N. N. Shefov and Yarin, V. I. : 1962, 'Atlas of the Airglow Specrtum 3000–12400 Å', *Planet. Space Sci.*, **9**, 883-915.

Mies, F. H. : 1974, 'Calculated Vibrational Transition Probabilities of $OH(X^2\Pi)$', *J. Molecular Spectroscopy*, **53**, 150-188.

Omholt, A. : 1971, 'The Optical Aurora', *Springer–Verlag Berlin Heidelberg: New York.*

Reasoner, D. L., Eather, R.H. and O'Brien, B. J. : 1968, 'Detection of α–Particles in Auroral Phenomena', *J. Geophys. Res.*, **73**, 4185.

Søraas F., Torheim, P., Aarsnes K. and Måseide, K. : 1989, 'Calculated and measured height variations of Doppler shifted hydrogen emissions at arbitrary angles with the magnetic field', *Scientific / Technical Report*, **217**, 1-12.

Vallance Jones, A. : 1974, 'Aurora', *D. Reidel Publ. co.: Holland.*

Van Zyl, B. and Neumann, H. : 1980, 'H_α and H_β Emission Cross Sections for Low–Energy H and H^+ Collisions With N_2 and O_2', *J. Geophys. Res.*, **85**, 6006.

van Rhijn, P. : 1921, 'On the brightness of the sky at night and the total amount of starlight', *Publ. Ast. Lab. Groningen.*, **31**, 1-83.

Vegard, L. : 1939, 'Hydrogen showers in the auroral region', *Nature: Lond.*, **144**, 1089.